LATVIAN JOURNAL of PHYSICS and TECHNICAL SCIENCES

ISSN 0868 - 8257

1

(Vol. 56)

2019

SATURS

ENERĢĒTIKAS FIZIKĀLĀS UN TEHNISKĀS PROBLĒMAS

KVANTU FIZIKA

CONTENTS

PHYSICAL AND TECHNICAL ENERGY PROBLEMS

QUANTUM PHYSICS

СОДЕРЖАНИЕ

ФИЗИКО-ТЕХНИЧЕСКИЕ ПРОБЛЕМЫ ЭНЕРГЕТИКИ

КВАНТОВАЯ ФИЗИКА

LATVIAN JOURNAL of PHYSICS and TECHNICAL SCIENCES

LATVIJAS FIZIKAS un TEHNISKO ZINĀTŅU ŽURNĀLS

ЛАТВИЙСКИЙ ФИЗИКО-ТЕХНИЧЕСКИЙ ЖУРНАЛ

Published six times a year since February 1964
Iznāk sešas reizes gadā kopš 1964. gada februāra
Выходит шесть раз в год с февраля 1964 года

1 (Vol. 56) • 2019

RĪGA

INDEKSĒTS (PUBLICĒTS) | INDEXED (PUBLISHED) IN

www.scopus.com
www.sciendo.com
EBSCO (Academic Search Complete, www.epnet.com), INSPEC (www.iee.org.com).
VINITI (www.viniti.ru), Begell House Inc/ (EDC, www.edata-center.com).

Izdevēji: Fizikālās enerģētikas institūts, LU Cietvielu fizikas institūts
Reģistrācijas apliecība Nr. 000700221
Redakcija: Krīvu iela 11, Rīga, LV-1006
Tel. 67551732
e-pasts: ezerniec@edi.lv
Interneta adrese: www.fei-web.lv

sciendo

LATVIAN JOURNAL OF PHYSICS
AND TECHNICAL SCIENCES
2019, N 1

DOI: 10.2478/lpts-2019-0001

PHYSICAL AND TECHNICAL ENERGY PROBLEMS

CATEGORISATION OF ANCILLARY SERVICES FOR PROVIDERS

J. Ehnberg[1]*, O. Lennerhag[2], E. Hillberg[3], A. Perez[4], A. Mutule[5], I. Zikmanis[6]
[1]Chalmers University of Technology,
Electrical Engineering,
11 Hörsalsvägen, Göteborg, 417 56, SWEDEN
[2]Independent Insulation Group,
5 Storgatan, Ludvika, 771 30, SWEDEN
[3]RISE Research Institutes of Sweden,
4 Brinellvägen, Borås, 504 62, SWEDEN
[4]ABB,
12 Ludvikavägen , Ludvika, 771 31, SWEDEN
[5, 6]Institute of Physical Energetics,
11 Krivu Str., Riga, LV-1006, LATVIA
*e-mail: jimmy.ehnberg@chalmers.se

The focus of the work presented here is to raise awareness of how ancillary services within the NordPool area could be of value in supporting the future grid, and who could be the provider of these services. The ancillary services considered here are not limited to the current market, but also services for future market solutions as well as services for fulfilment of grid codes. The goal is to promote the development of existing and novel solutions to increase the utilisation and thus the value of equipment within the power system. The paper includes a techno-economical categorisation of ancillary services, from a provider's perspective, presenting opportunities and competition. Furthermore, procurers of services could utilise this kind of categorisation to identify possible providers or partners. The analysis of the categorisation shows a broad range of possible providers for each service and a broad range of possible services from each provider.

Keywords: *ancillary services, black start, congestion management, frequency support, islanding, power quality, provider, stability, system restoration, voltage support*

1. INTRODUCTION

Ancillary services can be defined in many ways but are often considered as the services and functions necessary to support the secure and reliable operation of the

power system. These services have varying technical specifications and regulatory frameworks across the world, mainly influenced by the individual deregulation processes that have taken place in different countries [1]. Ancillary services have traditionally been provided from the centralized electricity production side, but in the future, other sources, such as Distributed Energy Resources (DER) and loads, are expected to provide these services to ensure a sustainable and reliable power supply for all levels in the grid. Ancillary services are still commonly provided by generators but to some extent also by loads and other network devices [2].

The European Network of Transmission System Operators for Electricity (ENTSO-E) [3] defines ancillary services as:

"…the range of functions which TSOs contract so that they can guarantee system security. These include black start capability (the ability to restart a grid following a blackout); frequency response (to maintain system frequency with automatic and very fast responses); fast reserve (which can provide additional energy when needed); the provision of reactive power and various other services".

The Federal Energy Regulation Commission (FERC) [4] defines ancillary services as:

"the services necessary to support the transmission of electric power from seller to purchaser, given the obligations of control areas and transmitting utilities within those control areas, to maintain reliable operations of the interconnected transmission system. Ancillary services supplied with generation include load following, reactive power-voltage regulation, system protective services, loss compensation service, system control, load dispatch services, and energy imbalance services".

In [5], the Union of the Electricity Industry (EURELECTRIC) defines ancillary services as:

"all services required by the transmission or distribution system operator to enable them to maintain the integrity and stability of the transmission or distribution system as well as the power quality".

The definitions of ancillary services have some coherence but there are small differences which could make it hard to get an understanding of what they actually are and if you could provide this kind of services. The differences in categories could stem from independent market deregulation in different parts of the world, which do not follow a common approach, as well as there are differences in the power system structures and available resources [1]. This might be a specific problem for future providers that are today not active in the power area, which is a target group at least according to the FERC that specifically addresses load dispatch and energy imbalance services.

A power system that could meet the paradigm shift that is expected in the grid with a high level of intermittent renewable energy sources [6], [7], converter-based resources [6] and load is needed. However, this does not only create the paradigm shift and its challenges, they can also be part of the solution [6], [7]. The possibilities for a limited number of providers and battery system to mitigate frequency and voltage stability issues are discussed in [6]. A similar categorisation to the one provided in this paper is presented in [7] and is based on the time-scale of the different ancillary services. However, it has a focus on thermal power plants and storage technologies

and the connection to specific present and future services is limited.

Storage technologies as providers of ancillary services are discussed in [8] and the paper shows which technology is suitable for which ancillary service. Another possible provider of ancillary services is a different type of load, often called demand response. A review of different types of demand response regimes is presented and the possibility to intervene with the grid is demonstrated in [9]. The review is based on different hieratical levels of power system studies (HL1 to HL3), which gives a good overview of the problem but has limitation to evaluate new opportunities to provide services.

There is an increased interest by new actors in the grid business; more people see and want to see more opportunities, for example, owners of distributed generation [10]–[12], battery system [11], [13] and loads, either individual or as virtual power plant (VPP) [10], [12], [14], [15]. The focus is mainly on participating in different types of the markets based on active power with a specific focus on energy and energy markets. However, there is also opportunity with more local focus by creating energy markets on distribution levels [12], [13]. Ideas of participation in frequency control and restoration also exist with well-developed bidding strategies [10] and evaluation of their economic benefits [11]. Creating VPP, by the use of, for example, aggregators, is one way to utilise also the benefits from small consumers, and opportunities are well identified at least for short-term electricity markets [14], [15]. More direct involvement is also proposed using intelligent loads (IL) [12]. By having this infrastructure in place, the step towards a more extensive participating of DG, VPP and IL into providing more ancillary services is not long. It is necessary to know more about the possibility.

The technical possibility to provide an ancillary service is today the only requirement to be a provider. Another crucial factor could be competitiveness with other providers, in terms of cost, but also with minimum impact on the environment and society. The economical evaluation can be based on an open market, which is already available for some of the services, but for many this is not the case. The other two dimensions of sustainability (i.e., environment and society) are more difficult to assess and, therefore, they are only generally addressed. In some cases, these dimensions are related to the economic area via, for example, diverse types of CO_2 taxes.

The goal of the paper is to illustrate the existing and probable future ancillary services from a provider's perspective.

2. GOAL OF THE PAPER

The goal of the paper is to provide a tool in order to evaluate which ancillary services can be provided by whom, from a perspective of owners of different power equipment, the so-called providers.

First, providers can identify the services they can provide. To some extent, they could also identify which services are closer to implementation than others. This is of extra importance to involve relatively new and future actors to provide ancillary services (e.g., hydrogen producers).

Second, a potential provider can see what kind of competitors they have for a certain service. This will not only determine the future price, but also which opportunities will appear at all. Since some services are more local than others, then the location of the competitors is also of importance.

Finally, the categorisation may be used to identify suppliers for someone that has the need for a certain service, e.g., fulfilment of grid codes, like reactive power compensation and harmonics mitigation, or for internal processes. This could lead to large benefits since the internal costs could be compared with the costs from an external supplier.

A larger range of providers of ancillary services could also have great environmental benefits because less equipment in general is needed. Less equipment means less material and, therefore, both environmental and economic dimensions are beneficial.

The procedure of evaluating different perspectives is out of the scope of this paper but a standard method can be expected to be used, perhaps depending on local and political circumstances.

The paper focuses on the NordPool area because markets of the ancillary services are by nature restricted to only one area. It also reduces the complexity to describe different services.

However, despite the focus in this study the categorisation can easily be translated to all other areas with some minor updates. Mainly updates on the ancillary services are needed to meet the local requirements. However, a review of the mapping might also be needed to make sure it matches the service.

3. ANCILLARY SERVICES

There is some ambiguity when finding a common categorisation for ancillary services, which can lead to confusion. According to [2], ancillary services have evolved to include new types of ancillary services, for instance, those that can be provided by renewable sources such as wind and solar power. Furthermore, the terminology used follows closely the terminology given by the ENTSO-E network codes. The authors found that three main groups of ancillary services could be pointed out, these being ancillary services related to: (1) frequency control, (2) voltage control, and (3) system restoration.

Report [2] also mentions an emerging ancillary service associated with renewable energy sources, more specifically wind power. This type of ancillary service would be focused on providing back-up and other services to the system operators, to counteract the stochastic behaviour of the wind power generators.

Therefore, the services are divided into four categories: frequency support, voltage support, system restoration and other services. Each service is described shortly, mainly based on the provider of today. The market for each service, if such exists, is described based on at least an existing market structure to exemplify. If no market is known, a common method to provide the service is described and market structure is proposed. If the service is dependent on localization of the provider, it is marked with an L in the overview table on the mapping.

3.1. Services Related to Frequency Support

3.1.1. Overview

Frequency in power systems is a system indicator of the balance between generation and consumption of electricity. Furthermore, frequency is tightly coupled to the active power in such a way that an excess in the active power input results in an increase in frequency, and vice versa. Loads and equipment such as induction motors and transformers are sensitive to frequency changes. For instance, frequency drops are known to cause high magnetizing currents in devices [16]. However, the indirect consequences may be much larger and even a threat to the operation. In classical power systems, the frequency is sustained by means of control systems through the governor of synchronous generators in the same synchronous area. However, with the phase-out of some conventional generation resources, enforced by market liberalization and/or environmental concerns, the share of non-synchronous converter-based generation has increased considerably.

3.1.2. Frequency Containment Reserve (FCR)

The purpose of the FCR is to stabilize the system frequency. In the NordPool countries, the FCR has been split into FCR-N for normal operation (50 Hz ± 100 mHz), and FCR-D for disturbance operation (49.9–49.5 Hz) [17]. The FCR control tasks are commonly referred to as primary frequency control.

FCR takes place as a joint action of the participating generating units within the synchronous area. It is provided through the turbine governors, with local and decentralized control, giving a fast and automatic response. According to [8], FCR should follow two main principles: (1) bring the rate of change of the frequency deviation to zero, and (2) the FCR available capacity shall be fully activated at the maximum steady-state frequency deviation.

Generally, the full activation time of FCR-D is between 0 and 30 seconds, sustaining up to 15 minutes, after which it is released [2]. According to the survey presented in [1], the deployment start of the FCR is instantaneous, and it is fully committed in less than 30 seconds in most EU countries. In the NordPool area, 50 % of FCR-D shall be active within 5 seconds, and it shall deliver its full response within 30 seconds [18]. On the other hand, since FCR-N is within normal operation mode, its activation is slower compared to the FCR-D, i.e., FCRN is activated within two to three minutes [18].

The providers of FCR are today generators equipped with a speed governor. The demand side also participates in this control due to the self-regulation of frequency dependent loads such as directly connected induction motors and loads equipped with under frequency relays; however, loads are rarely considered as part of the frequency regulation [1]. In the NordPool area, automatic load shedding is not part of the FCR, but instead considered as system protection for disturbances where the FCR-D has been unsuccessful to prevent the frequency to drop below 49.5 Hz [19].

In addition, it is technically possible to provide FCR by HVDC connections between neighbouring synchronous systems. Such frequency-controlled regulation of HVDC may be referred to as emergency power and is in the NordPool area [17] considered partly within the FCR-D and partly as system protection to mitigate disturbances below 49.5 Hz [19].

Market Related Aspects

FCR is a market product procured by the TSO. There are several procurement methods in electricity markets, including compulsory provision, bilateral contracts, tendering process, and spot market. In the NordPool area, the FCR (FCR-N and FCR-D) is obtained through a tendering process [20]. The generation companies can submit their FCR-N/D bids one or two days ahead the operational day. The bids can be longer than one hour, but still limited to a number of consecutive hours, for instance, six hours for the bids submitted two days before, and three hours for the day ahead bids [21].

The payment method can be regulated price, pay as bid resulting from a tendering process, common clearing price resulting from a spot market, or non-remunerated. In the NordPool area, the remuneration method is pay as bid. In most cases, the TSOs pay for the product availability, but in some cases, a frequency utilization payment is also added [20].

3.1.3. Frequency Restoration Reserve (FRR)

The FRR process aims at restoring the frequency back to its nominal value by activating the reserves within a predefined time [22], by modifying the set point of reserve-providing units [2]. FRR also aims at replacing the FCR reserves. The control tasks related to FRR are commonly referred to as secondary frequency control.

The activation process can be either automatic (aFRR, delivered from spinning reserve) or manual (mFRR, delivered from spinning and standing reserve). FRRs are managed by the TSO [2].

A synchronous area may contain several load-frequency control areas (LFC area), e.g., delimited by countries. In such cases, the Area Control Error (ACE), which is defined as the difference between the scheduled and actual power flows for an area, helps determine the participation factor of that area in the frequency restoration process [22]. As mentioned in [1], every area is responsible for maintaining its load and generation. This means that the flows in and out the area should be restored by FRR, bringing the ACE to zero.

Only generating units located in the same LFC area from where the imbalance originates should participate in this control (normally it is the responsibility of each LFC area to keep its load and generation in balance) to avoid unplanned power flows. Loads do not participate in this control [1].

Market Related Aspects

The most common procurement methods for FRR are bilateral contracts, tendering processes, and spot market. Reported payment methods are pay as bid and common clearing price. Furthermore, the remuneration structure is based on availability and utilization, as it is inherent from the previously mentioned procurement methods [20].

3.1.4. Replacement Reserve (RR)

Replacement reserves (RR) are defined in [23] as follows:

"the active power reserves available to restore or support the required level of FRR to be prepared for additional system imbalances, including operating reserves".

The RR replaces utilized FRR-reserves, helps manage congestions in the transmission network, and brings the frequency and the interchanges back to their target values when FRRs are unable to perform this task [1]. RRs are activated manually and centrally at the TSO control centre [2], i.e., through manual changes in the dispatching and commitment of generating units.

The service deployment time varies widely among TSOs. Non-synchronous resources are treated differently in this service [1]. According to the CIGRE global survey presented in [24], the RR ("Tertiary Control Tasks") timeframe is generally 30 to 120 minutes.

Market Related Aspects

Some aspects of RR are related to trading for energy balancing purposes, which is not a service provided by the system users to the TSO and hence not an ancillary service, i.e., balancing takes place among the system users in the electricity market that aims "to balance their financial positions" [20].

The remuneration structure of this ancillary service is pay as bid in most systems [20]. Availability and utilization payments are the most common remuneration structures. In some markets, fixed and utilization frequency payments exist, for instance, in Great Britain. Opportunity cost payments are rarely seen, since these are hard to compute [20].

3.1.5. Fast Frequency Response (FFR)

FFR can be achieved by rapid injection of active power or reduction of load, in a timeframe so that it can arrest a frequency decay, i.e., decreasing the Rate of Change of Frequency and the nadir, giving sufficient time to activate the FCR [25]. FFR has been proposed to be available within 2 seconds and sustained for at least 15 seconds [26].

Possible providers of FFR are conventional generators, loads with under frequency relays, synchronous storage units like pumped hydro, HVDC interconnectors

to other power systems, doubly-fed induction generators (DFIG) and full converter-based wind turbines [2], as well as energy storage systems (ESS) [18].

FFR can be in the form of real inertia from rotating mass or emulated by power electronics-interfaced power sources. Moreover, the emulated response is commonly referred to as synthetic inertia.

Market Related Aspects

Currently, FFR does not exist as a product on the electricity market. Some system operators have proposed the introduction of this ancillary service in their system, for instance, in the Electric Reliability Council of Texas (ERCOT) power system. According to ERCOT's concept paper on future ancillary services [25], the market considerations of a suggested Synthetic Inertia/FFR ancillary service can be summarised as follows: First, the required amount of inertia is determined, which later would be acquired through a Residual (alt. Reliability) Unit Commitment (RUC) process. Normally, the RUC process precedes the Day Ahead Market (DAM), and during the RUC process the day ahead schedule resulting from the DAM remains locked, i.e., the units committed in the DAM are considered as "must run" during the RUC process [27]. Provision of FFR ancillary service under the aforementioned structure implies that resources aiming at provision of FFR/Synthetic Inertia would necessarily have to participate in the DAM. Moreover, the total amount of RUC awarded in the system is normally limited by the total energy bid minus the day ahead scheduled energy plus the upward ancillary services (resulting from the DAM) [27].

3.2. Services Related to Voltage Support

3.2.1. Overview

For electrical equipment to function properly, the supply voltage must be within certain required values; hence, actions should be taken to fulfil this requirement. While frequency is a system wide parameter, voltage is a local quantity tightly coupled to the reactive power injection to network nodes [2] and thereby a more local parameter. The measures can be performed in steady state or in dynamic operation mode [2].

3.2.2. Normal Operation: Power Factor-, Reactive Power- and/or Voltage-Control

The aim of this ancillary service is to control the voltage level of the network nodes. This is achieved by injecting or absorbing reactive power at the voltage controlled node, so that the voltage is kept within acceptable margins. In general, the technical requirements of this service are principally concerned with the absorption and production of reactive power, expressed in fractions of the nominal active power at the point of delivery [1]. The timeframe of operation is within hours [2], with immediate deployment time, and continuous operation to keep the voltage at its nominal and ensure stability [1].

Providers of this service are, e.g., synchronous sources, static compensation, SVCs, tap changing transformers, transmission lines (by switching), virtual power plants, demand facilities, and load shedding [2]. Devices interfaced to the grid through power electronic converters, such as wind turbines, PV, and HVDC-VSC links, can also provide this service.

Market Related Aspects

Provision of this service is compulsory and regulated in the grid codes. The services are non-remunerated in most systems, but bilateral contracts and tendering process have been reported in some countries, with regulated and pay as bid payments [20]. When present, the remuneration method is fixed or for availability. Due to the local nature of voltage, this ancillary service is prone to the exercise of market power [20].

3.2.3. Fast Reactive Current Injection

Fast reactive current injection can be defined as the capability of a generator to provide a proportionate response to a voltage dip [2]. Some possible specifications for this ancillary service could impose requirements on the delivered response, e.g., rise time, overshoot, and settling time [26].

It aims at controlling the voltage in a dynamic timeframe from tens of milliseconds to minutes, enhancing the dynamic security of the system, e.g., in order to prevent voltage collapse, or to limit it to some extent. It also helps with other voltage quality issues [2].

The providers of this service could be synchronous generators [26], reactors and capacitors, SVCs, VSC-HVDC substations, FACTS devices [2] and other converter-based providers such as wind power plants, PV systems, and energy storage systems (e.g., batteries).

Market Related Aspects

Currently, there is no market structure in place for fast reactive current injection, but it is demanded in some grid codes. A suggestion given in [20] is that there should be a change in the mind-set regarding how this kind of service should be remunerated to reduce the system cost. This could be done by allowing the local provider with the lowest cost to provide the service.

3.3. Services Related to System Restoration

3.3.1. Black Start

Black start is defined as the set of actions aimed at bringing the system back to normal operation after disturbance that caused a blackout or state of emergency.

It is carried out sequentially: 1) re-energization, 2) frequency management, and 3) re-synchronization [2].

Providers of this service are normally neighbouring TSOs by means of tie lines, and alternatively internal resources having black start capabilities, i.e., resources capable of controlling voltage and speed/frequency in a stable islanded mode [2].

Market Related Aspects

In the NordPool system, the capacity is directly procured based on system needs of the TSO.

3.3.2. Islanding

The requirements for islanding are similar to those of Black Start but the duration is longer. Maintaining generation-demand balance is the first-hand requirement for stable islanding operation. The generators in the island must be able to maintain the voltage and frequency. In addition, the generators should be able to keep the network impedance within range, the phase symmetry, the ability to handle fault currents, and the resynchronization with the rest of the network [2].

In a sense, all power systems are islanded. However, this does not mean that every generator can provide stable islanded operation by itself. One example is intermittent sources such as PV, which may very well function in a smaller islanded system, but they need additional generating sources or storage, e.g., during night-time to provide a stable islanding operation.

Market Related Aspects

Currently, there is no market structure in place but the capability is regulated in some grid codes. The service is little more complicated since it can be hard to predict in what ways the system will split. A more dynamic market is proposed, since islanding occurs relatively seldom, and the market needs to be based on available resources rather than special installations. A fix feed-in tariff and thereby fix cost could also be a market solution to get a predictable system in an emergency situation.

3.4. Other Services

3.4.1. System Stability Services

One type of system stability service is Power Oscillation Damping (POD). The basic principle of POD is that active or reactive power is used to counteract oscillatory behaviour in the system.

Current providers of this service are, e.g., synchronous generators equipped with a Power System Stabilizer (PSS), STATCOMs, VSC-HVDC stations, and other FACTS devices. Some possible future providers of stability services are wind farms connected to the transmission network [28].

Market Related Aspects

Some TSOs have established (or may establish in the future) in their grid codes that non-synchronous generation, such as wind farms, should provide frequency and reactive power regulation ancillary services. Furthermore, capabilities for the damping of power system oscillations may also be required [28]. Remuneration could be based on what extra cost can be added for removing this kind of requirement in the grid codes.

3.4.2. Power Flow/Congestion Management

Power flow management is basically a network planning related issue. This service also includes peak shaving/energy arbitrage, demand side flexibility, and load management.

Some possible providers of a power flow/congestion management ancillary service are, e.g., phase shifting transformers, on-load tap changers at substations, supplementary line regulators on feeders, switched capacitor banks at low voltage/ medium voltage substations, and coordinated reactive power injection of DG connected at the DSO level. The opportunities might increase for DG in the future due to a higher collective availability [2].

Providers of peak shaving/energy arbitrage could be, e.g., Battery Energy Storage Systems (BESS). The peak shaving and energy arbitrage capabilities offered by BESS have been demonstrated, e.g., in [29]. However, the companion paper [30] showed that the analysed BESS were not economically feasible without subsidy capital at the current battery prices (year ~2016).

Providers of demand side flexibility could be industrial, residential and commercial loads. Demand side flexibility of commercial buildings based on the coupling of the inherent thermal energy storage characteristics of the building to the grid, by means of the heating-ventilation-and-air-conditioning systems, has been studied in [31]. The services provided by buildings include scheduling of price-sensitive load and load shifting (basically energy arbitrage).

Market Related Aspects

At the TSO level, there is the market dealt with in the energy market by, e.g., counter purchases. However, no such markets exist at the DSO level. Energy market at the distribution level can be implemented, access to smart meter data could be a key factor. The focus should be placed on adapting loads rather than production; virtual power plants could be used to implement the system by the use of aggregators.

3.4.3. Power Quality Services

Power quality services could include, e.g., harmonic mitigation. The basic principle of harmonic mitigation is that a harmonic component is imposed on the

delivered current, e.g., in order to counteract an existing distortion in the grid. It could also be provided as coordination between, e.g., several wind turbines, where the phase angle is adjusted to minimise the harmonic current for each harmonic order, thereby limiting the total harmonic distortion at the point of connection [32].

Market Related Aspects

Currently, there is no market structure in place, but most grid codes include requirements on the harmonic emissions at the point of connection. A market based on fulfilling other grid codes is possible, but it requires the DSO to have a more open view on where in the grid the codes need to be fulfilled.

4. PROVIDERS OF ANCILLARY SERVICES

A mapping of ancillary services has been done from the perspective of which services a certain type of providers may contribute. The mapping also includes the colour coding used for this techno-economic consideration as can be seen in Table 1.

Table 1

The Techno-Economic Categorisation of Ancillary Services Using the Following Colour Code

Currently utilised, technically and commercially feasible	G
Technically possible with minor modifications; Assumed smaller investments and/or close to commercially feasible (with respect to its present commercial setup and operation)	Y
Technically possible with major modification; Assumed larger investments and/or distant to commercially feasible (with respect to its present commercial setup and operation)	R
Technically not applicable/possible and/or assumed economically infeasible	N/A

In Table 2, the mapping of ancillary services is presented for a list of different types of providers. This table also includes information regarding the importance of location of the provider of ancillary services.

The used numeral interpretation list for Table 2:

1. This is provided naturally through the inertial response of the generator.
2. While it is not used in Sweden, nuclear power is used in, e.g., France for freq. support.
3. This is part of the regulations for production units, it is not monetized.
4. This is normally only possible for down-regulation or if it is normally not producing the maximum available output.
5. In many cases, this is dependent on the converter rating. If the converter is not rated for higher capacity needed for continuous reactive support, this will not be possible during full production.
6. It may be possible for an arc furnace to contribute to lower flicker levels based on adjustments of the process.
7. More complex to realize since aggregator might be needed.

Table 2

Technical and Economical Categorisation of Ancillary Services from Different Types of Providers

	FFR	FCR	aFRR, mFRR	RR	Fast reactive current injection (L)	Slow PF, U,Q control (L)	Black start (L)	Island-ing (L)	System stability services (L)	Conges-tion manage-ment (L)	Other PQ services (L)
Hydro power (run of river)	G, 1)	N/A	N/A	N/A	Y	Y	G	G	G	G	R
Hydro power (w. reservoir)	G, 1)	G	G	G	Y	G, 3)	G	G	G	G	R
Nuclear	G, 1)	Y, 2)	Y, 2)	G	Y	G, 3)	N/A	N/A	G	G	R
Gas/oil	G, 1)	G	G	G	Y	G, 3)	G	G	G	G	R
Waste	G, 1)	G	G	G	Y	G, 3)	G	G	G	G	R
Biomass	G, 1)	G	G	G	Y	G, 3)	G	G	G	G	R
Classic HVDC	Y	G	Y	Y	N/A	Y	R	R	R	G	R
HVDC-VSC	Y	G	Y	Y	G	Y	G	G	G	G	Y
PV	Y, 4)	R	R	R	R	Y	R	R	Y	G	Y
Wind	Y, 4)	R	R	R	G	Y, 5)	R	R	Y	G	Y
Wave tidal	Y, 4)	R	R	R	G	Y, 5)	R	R	Y	G	Y
Pumped hydro	G	G	G	G	G	G	G	G	Y	G	R
CAES	G	G	G	G	Y	Y	G	G	Y	G	R
H_2 storage	G	G	G	G	Y	Y	G	G	Y	G	G
BESS	G	G	G	G	Y	Y	G	G	Y	G	G
Flywheel	G	N/A	N/A	N/A	Y	R	R	R	Y	G	R
Thermal	G	G	G	G	Y	G	Y	Y	Y	G	G
Super-capacitors	G	N/A	N/A	N/A	Y	R	R	R	Y	G	R
Industry	G, 1)	Y	Y	Y	R	R	N/A	Y	Y	Y	R, 6)
Commercial buildings	Y, 7)	Y, 7)	Y, 7)	Y, 7)	R, 7)	R, 7)	N/A	Y, 7)	Y, 7)	Y, 7)	R, 7)
Household	Y, 7)	Y, 7)	Y, 7)	Y, 7)	R, 7)	R, 7)	N/A	Y, 7)	Y, 7)	Y, 7)	R, 7)

(L) represents the importance of localization of the provider of the ancillary service (for other services, the provider is only required to be located in the same synchronous system unless transmission between the system is possible, then the scope is even broader). The letters in the cells are only an indication of the colour.

In Table 2, presumed providers can easily see what kind of ancillary services they have the possibility to provide by examining the row they are in. Based on information in the table, the provider will need to conduct more thorough investigation on the supply of a specific service due to local circumstances, such as grid limitation or other operating conditions. The table just provides a guidance on where to start developing business.

In columns for each service the competition between services can be examined. This information can be used to evaluate the value of participation.

Fast frequency response can be provided by a wide range of providers. However, some of them will require software updates. Very little loss of electricity

production or additional losses are expected, which makes several of them possible and suitable providers. The relative need in the system is not expected to increase in the future but the capacity of some of the current providers is expected to decrease, which will create an additional need.

For the other frequency response services such as FCR, aFRR, mFRR and replacement reserves, the situation is quite similar and can be provided by many more providers than today. Some of the providers might require some control system updates and write the business contracts to the able to participate in the existing market(s). Renewable electricity technologies can provide the services, but they cannot up-regulate without losing production and their often intermittent behavior makes them sometime not available, not even for the down-regulating. The relative need of the system is not expected to increase, or maybe even decrease due to the trend of more and smaller production units. However, capacity of providers of today are expected to decrease more and faster than the need and will therefore create an additional need.

Reactive power/voltage and power factor control both fast and slow can also be provided by many providers but many of them will require some control system updates especially for the fast control. The production or consumption is dependent of the nominal power rating rather than active power provided, which gives opportunities. Therefore, there might be a need to increase the rating of generators or converters, depending on the type of provider, to avoid loss of any electricity production. The relative need of the service will probably not increase except in the distribution system where it probably will increase, due to a more complicated electricity consumption and production pattern in the future. Some of the large providers of today might not be available and, therefore, it can be concluded that more capacity is going to be needed in the future.

More providers of black start capability and islanding are available today. More providers of these services will increase the possibility of operation during outages or increase the speed for rebuilding the power system after extensive outages, which could have a major positive impact on the society as a whole. Especially islanding would provide the possibility to increase the production over time since less stops will be required due to grid problems. Black start and islanding are services that seldom if ever are used due to the high reliability in the system. However, the need for them will probably increase in the future due to more intermittent production, which will give a more complicated operation situation and, therefore, there will be a risk for more outages. The need will probably also increase due to higher demand from electricity access in the society as a whole. Current providers will then not be enough and might not be in the correct location due to other changes in the society and, therefore, there will be an increased need also for new providers of these services in the future.

System stability services can be offered by many providers, but the location in the system is important and control system updates are in most cases needed. The electricity production and consumption of the provider will hardly be affected by provision of the service, which will increase the interest of participation.

Congestion management can be done by all providers; however, it needs to be implemented in different ways depending on the type of provider. By access to the

service, the utilization rate of the system could go up even if losses increased and there might be limitation to provide renewables into the system on some occasions. Congestions are expected to increase due to the expected new more complicated consumption and production pattern, especially at lower voltage levels where new providers are required due to a lack of existing providers.

PQ services can mainly be provided by converter connected providers (except classical HVDC). Providing the services will increase the need of capacity and will only have limited impact on active power exchange, in an equivalent way as reactive power control. These services could reduce losses in the system and even prevent shorting of the expected lifetime of equipment. Since the number of the components in the system creating PQ issues will increase, there will be an increased need for these kinds of services in the future.

If a provider is investigating the possibility to provide multiple services, the competition between services needs to be studied to assess the risks of not providing the actual service when required.

Depending on the nature of the issues that the service addresses, the physical location of equipment may need to be investigated. For services marked with an (L), the location in the grid is of importance while the other services are system based. It should be noted that the location in the grid may differ from the geographical location. Since grid is often based on different zones, it might be not possible for the provider to offer the service. This problem is most common in services related to distribution systems and especially at low voltage levels, such as voltage control, congestion management and other PQ services as described in Table 2.

An additional application of this categorisation is to identify providers of certain services for a service procurer, either from a system responsibility party, such as TSO or DSO, or from other parties who could benefit from external support, e.g., to fulfil grid codes.

5. CONCLUSIONS

Categorisation of ancillary services is proposed to provide an evaluation tool of participation for the present and future actor in the power business. This is made to counteract the ambiguity in the terminology used regarding ancillary services, which might inhibit the development of ancillary services. A common terminology could ease the work by explaining a wider range of providers of ancillary services in order to get higher diversity of providers in the system.

By examination of the categorisation, any need for investments are indicated. The examination is based on the type of provider. In the market, there is also knowledge about competition that is crucial to avoid being ousted. For services that currently have no markets, the categorisation can be used to find suppliers. This could be useful not only for TSOs and DSOs but also for those that have challenges in fulfilling certain grid codes.

The analysis has shown that there will be more opportunities for renewable energy sources and other equipment connected to the electric grid to provide more ancillary services. However, there might be some need for hardware and/or software

updates. Providing more ancillary services could achieve a decrease in cost and/or negative environmental and social impact of these services and thereby decrease the impact of the power system on the society in the near future.

ACKNOWLEDGEMENTS

The research has been supported by Smart Grids Plus ERA-Net project CLOUDGRID No.77547 (Transnational CLOUD for Interconnection of Demonstration Facilities for Smart GRID Lab Research & Development). This project has received funding in the framework of the joint programming initiative ERA-Net Smart Grids Plus, with support from the European Union's Horizon 2020 research and innovation programme.

REFERENCES

1. Rebours, Y. G., Kirschen, D. S., Trotignon, M., & Rossignol, S. (2007). A survey of frequency and voltage control ancillary services – Part I: Technical Features. *IEEE Transactions on Power Systems, 22*(1), 350–357.
2. H. Holttinen, Cutululis, N. A., Gubina, A., Keane, A., & Van Hulle, F. (2012). Ancillary services: Technical specifications, system needs and costs. *Deliverable D 2.2. REserviceS project*.
3. ENTSO-E. (2015). *Balancing and Ancillary Services Markets.* ENTSO-E. [Online]. [Accessed: 10 September 2018] https://docstore.entsoe.eu/about-entso-e/market/balancing-and-ancillary-services-markets/Pages/default.aspx
4. Federal Energy Regulatory Commission. (2016). Glossary. [Online]. [Accessed: 10 September 2018] https://www.ferc.gov/market-oversight/guide/glossary.asp
5. EURELECTRIC. (2004). Ancillary Services. Unbundling Electricity Products – An Emerging Market. *EURELECTRIC Thermal Working Group*, Ref: 2003-150-0007.
6. Kroposki, B., Johnson, B., Zhang, Y., Gevorgian, V., Denholm, P., Hodge, B.-M., & Hannegan, B. (2017). Achieving a 100% renewable grid: Operating electric power systems with extremely high levels of variable renewable energy. *IEEE Power and Energy Magazine*, *15*(2), 61–73.
7. Alizadeh, M. I., Parsa Moghaddam, M., Amjady, N., Siano, P., & Sheikh-El-Eslami, M.K. (2016). Flexibility in future power systems with high renewable penetration: A review. *Renewable and Sustainable Energy Reviews*, *57*, 1186– 1193, ISSN 1364-0321.
8. Palizban, O., & Kauhaniemi, K. (2016). Energy storage systems in modern grids – Matrix of technologies and applications. *Journal of Energy Storage*, *6*, 248– 259, ISSN 2352-152X.
9. Jabir, H. J., Teh, J., Ishak, D., & Abunima, H. (2018). Impacts of demand-side management on electrical power systems: A review. *Energies*, *11*, 1050.
10. Mashhour, E., & Moghaddas-Tafreshi, S. (2011). Bidding strategy of virtual power plant for participating in energy and spinning reserve markets – Part I: Problem formulation. *IEEE Transaction on Power Systems*, *26*(2), 949–956.
11. Litjens, G.B.M.A, Worrell, E., & van Sark W.G.J.H.M. (2018). Economic benefits of combining self-consumption enhancement with frequency restoration reserves provision by photovoltaic-battery systems. *Applied Energy*, *223*, 172–187.

12. Chen, S., Ping, J., Le, X., Yan, Z., Xu, X., Yao, L., & Xi, J. (2018). Forming bidding curves for a distribution system operator. *IEEE Transaction on Power Systems*, *33*(5).
13. E. Stai, Reyes Chamorro, L. E., Sossan, F., Le Boudec, J.-Y., & Paolone, M. (2018). Dispatching stochastics heterogeneous resources accounting for grid and battery losses. *IEEE Transaction on Smart Grids*, *9*(6).
14. Nguyen, H., Le, L.B., & Wang, Z. (2018). A bidding strategy for virtual power plants with the intraday demand response exchange market using stochastic programming. *IEEE Transaction on Industrial Applications*, *54*(4).
15. Nguyen, H. & Le, L. (2018). Bi-objective-based cost allocation for cooperative demand-side resource aggregators. *IEEE Transaction on Smart Grids*, *9*(5).
16. Kundur, P., Balu, N. J., & Lauby, M. G. (1994). *Power system stability and control* (Volume 7). New York: McGraw-Hill.
17. ENTSO-E. (2016). *Nordic Balancing Philosophy*. ENTSO-E.
18. Moreno, O. J. (2017*). Ancillary Service for Frequency Support – Design of a Battery Storage Ancillary Service for Frequency Support in the Nordic Power System*. Master Thesis, Chalmers University of Technology.
19. ENTSO-E. (2017). *NORDIC System Operation Agreement – Appendices*. ENTSO-E.
20. Rebours, Y. G., Kirschen, D. S., Trotignon, M., & Rossignol, S. (2007). A survey of frequency and voltage control ancillary services – Part II: Economic features. *IEEE Transactions on power systems, 22*(1), 358–366.
21. Svenska Kraftnät AB. (2017). *Balance Responsibility Agreement*. [Online]. [Accessed: 14 September 2018] https://www.svk.se/en/stakeholder-portal/Electricity-market/Balance-responsibility/balance-responsibility-agreement/
22. ENTSO-E. (2013). *Supporting Document for the Network Code on Load-Frequency Control and Reserves for Electricity*, ENTSO-E.
23. European Commission. (2016). *Establishing a Guideline on Electricity Transmission System Operation – Draft*.
24. Cigré Working Group C5.06, TB 435. (2010). *Ancillary Services: An overview of International Practices*. Cigré.
25. ERCOT. (2013). *Future Ancillary Services in ERCOT – Initial Public Draft Version 1.0. ERCOT*.
26. EirGrid., & Soni. (2012). DS3: System Services Consultation – New Products and Contractual Arrangements.
27. Papalexopoulos, A. D., & Andrianesis, P. E. (2014). Day ahead energy market and reliability unit commitment: An integrated approach. *Power Systems Computation Conference (PSCC)*, Wroclaw, Poland.
28. Dominguez-Garcia, J. L., Gomis-Bellmunt, O., Bianchi, F. D., & Sumper, A. (2012). Power oscillation damping supported by wind power: A review. *Renewable and Sustainable Energy Reviews, 16*(7), 4994–5006.
29. Telaretti, E., & Dusonchet, L. (2016). Battery storage systems for peak load shaving applications: Part 1: Operating strategy and modification of the power diagram. In *IEEE 16th International Conference on Environment and Electrical Engineering (EEEIC)* (pp. 1996–2001), 7–10 June 2016, Florence, Italy.
30. Telaretti, E., & Dusonchet, L. (2016). Battery storage systems for peak load shaving applications: Part 2: Economic feasibility and sensitivity analysis. In *IEEE 16th International Conference on Environment and Electrical Engineering (EEEIC)* (pp. 2006–2011), 7–10 June 2016, Florence, Italy.

31. Kim, Y.-J., Blum, D. H., Xu, N., Su, L., & Norford, L. K. (2016). Technologies and magnitude of ancillary services provided by commercial buildings. *Proceedings of the IEEE, 104*(4), 758–779.
32. Abinava, M., Senthilnathan, N., & Sabarimuthu M. (2014). Harmonic compensation as ancillary service in PV inverter based residential distribution system. In *International Conference on Circuit, Power and Computing Technologies (ICCPCT),* Nagercoil, India.

SISTĒMAS PALĪGPAKALPOJUMA KLASIFIKĀCIJA PAKALPOJUMA SNIEDZĒJIEM

J. Ehnberg, O. Lennerhag, E. Hillberg, A. Perez,
A. Mutule, I. Zikmanis

K o p s a v i l k u m s

Elektrisko tīklu attīstība mūsdienās tiecas samazināt ietekmi uz vidi, attīstīt jaunas tehnoloģijas un inovatīvus risinājumus. Tīkla turpmākā attīstības gaita būtiski ietekmēs tīkla stabilitāti, tādejādi nākotnes tīklā paredzēta paaugstināta nepieciešamība pēc energosistēmas palīgpakalpojumiem.

Šobrīd palīgpakalpojumus var sniegt tikai tīkla dalībnieki, kuri atbilst pārvades tīklu izvirzītajām tehniskajām prasībām. Prasības spēj izpildīt lielie tīkla dalībnieki, toties liels potenciāls atrodams izkliedēto ģenerācijas avotu un dažādo veidu slodžu lokā. Šis potenciāls netiek pilnvērtīgi izmantots, kas saistīts ar informācijas trūkumu, terminoloģijas neskaidrībām un nestandarta pieejām. Izmantojot šos mazākos tīkla dalībniekus, ir iespējams sniegt palīgpakalpojumus ar jaunu pieeju.

Raksts klasificē tehniski ekonomisku informāciju par dažādiem sistēmu palīgpakalpojumiem no pakalpojuma sniedzēja puses. Apkopotā informācija sniedz informāciju par pakalpojuma realizācijas sarežģītības pakāpi, ieskatu potenciālajā konkurencē, iespēju dažādībā, lokācijas būtībā attiecībā no palīgpakalpojuma, kā arī ieskatu tirgus iespējās.

21.01.2019.

sciendo

LATVIAN JOURNAL OF PHYSICS
AND TECHNICAL SCIENCES
2019, N 1

DOI: 10.2478/lpts-2019-0002

OPTICAL PROPERTIES OF NEW TYPE OF GLAZING UNIT MODIFIED BY PHASE CHANGE MATERIAL (THEORETICAL APPROACH)

M. Vanags, K. Lebedeva, A. Snegirjovs, G. Kashkarova, P. Shipkovs
Institute of Physical Energetics
11 Krivu Street, Riga, LV-1006, LATVIA

The paper presents the use of phase change material (PCM) in window application that was studied in the framework of the ERA-NET-LAC Project "Solar Hybrid Translucent Component for Thermal Energy Storage in Buildings" (SOLTREN). Increase of energy savings in buildings is the main aim of this study. To achieve the aim, it has been decided to create a theoretical model of the impact of the PCM on the characteristics of the window and, at the next stage, to experimentally test the model. Paraffin has been chosen as the most suitable and available material as PCM. Pure paraffin has high transparency in liquid phase, and dull white colour in solid phase. The paper shows results of total transmittance and absorption spectra for different thicknesses of paraffin with a melting temperature of 35 °C, as well as absorption of the glass sample with PCM at different angles of incidence of light.

Keywords: *energy savings in buildings, optical properties, phase change material, window glazing*

1. INTRODUCTION

Most countries have significantly reduced their total energy use per unit of GDP over the past three decades. The decline in energy intensity has been driven largely by improved energy efficiency in key end-uses such as vehicles, appliances, space heating and industrial processes. Governments have implemented a wide range of policies and programmes such as energy efficiency standards, educational campaigns, obligations for market participants and financial incentives to accelerate the development and adoption of energy efficiency measures [1]. In this way, policies and programmes have helped improve energy efficiency and continue to develop technology in response to rising energy prices and increased competition in the energy sectors.

In all climatic conditions, it is very important to increase energy efficiency in buildings because in warm climate zones a high amount of energy is required for conditioning, but in cold climate zones for heat supply.

Most of the studies and applications have focused on the "opaque" part of

building envelopes, such as walls, ceilings, and floors. However, we should notice one fact: generally speaking, "transparent" part of the building envelopes, i.e., window has much lower thermal resistance than other parts of the envelopes [2].

From the thermal point of view, windows represent the weak link between the internal and external ambient zones of a room. In cold climates, they are responsible for 10 %–25 % of the heat lost from the heated ambient to the external atmosphere [3].

Many scientists are working on these problems, but energy efficiency measures should not only increase the energy efficiency of buildings, but also maintain an appropriate micro climate in their premises. Currently, there are commercially available types of glazing such as Delta®-Cool 28 or GlassX® that incorporates phase change material (PCM) (the PCM incorporated in the GlassX products is comprised of $CaCl_2 \times 6H_2O$ salt hydrates that are completely sealed in clear polycarbonate) [4]. The products have a latent thermal storage of up to 4268 kJ/m^2, meaning that a period of 8 h passes before heat is transmitted [5].

The paper describes an opportunity to develop a new type of glazing unit modified by phase change material to improve thermophysical characteristics of window component as an effective and unique type of a solar thermal energy storage system.

Considering physical characteristics, transparent or translucent building components like windows are the weakest elements of building envelope. Their U values are usually 4 times higher than for opaque ones causing considerable increase of heat loss during winter. In summer, relatively high solar transmittance is a source of undesirable heat gains, which result in overheating. At the same time, during the whole year the radiant asymmetry close to the window surface influences thermal comfort. On the other hand, glazing elements are necessary in buildings to provide the required amount of daylight, preferably in a diffuse form. Developed solar hybrid component would simultaneously ensure a sufficient illuminance level and stabilized thermal conditions by latent heat storage in the PCM layer.

The idea of refining thermophysical properties of glazing components, e.g., windows by PCM application is relatively brand new. However, some experimental and simulation analyses have been carried out up till now.

This concept of the PCM filled window system is viable and thermally effective. The PCM filling leads to filtering out the thermal radiation and reduces the heat gain or losses because most of the energy transferred is absorbed during the phase change of the PCM. The double glass window filled with PCM is more thermally effective than the same window filled with air [2].

To achieve the aim of the study, it has been decided to create a theoretical model of the impact of the PCM on the characteristics of the window and, as the next step, to experimentally test the model.

2. THEORETICAL MODEL

The first task of this model is to create a simplified measurement procedure for PCM light transmittance at different angles of the light source. The light transmittance

through the window in which the PCM is filled depends on the location of the Sun at the sky, or the angle of incidence of the light α from the window plane. Assuming that the solid state of the PCM is homogeneous, the light path d through PCM changes only from angle of incidence α (Fig. 1).

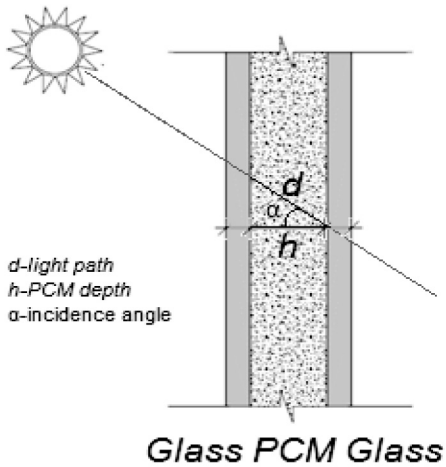

Fig. 1. Light path through the PCM to the angle of incidence.

Consequently, the light path d through PCM depending on the angle of incidence of light on a window plane can be expressed by the following formula:

$$d = \frac{h}{cos\alpha}, \tag{1}$$

where h is the gap thickness in which the phase change material is filled. This assumption allows us to study the optical properties of samples of different thickness of PCM and to express the thickness as the angle of incidence of the light source on the window plane.

The second task is to understand the influence of glass on the properties of light transmittance. In operation, the external glass receives solar radiation, where part of it is absorbed, part is reflected and the rest, about 80 %, is transmitted to the PCM region (initially in the solid phase) [6]. Light transmittance through glass, depending on the location of the light source, will not be significantly affected by the thickness of glass, but the reflection of light on the glass surface. Thus, it is experimentally necessary to determine light transmittance through a glass sample at different angles of incidence of light.

Knowing light transmittance through PCM samples of different thicknesses and knowing light transmittance through a glass sample at various angles and summing up the absorption of light in both materials and converting total absorbance into permeability, it is possible to obtain light transmission through a common system of glass-PCM glass.

3. EXPERIMENTAL SETUP

Paraffin samples were prepared according to the following scheme: one end of the stainless steel tubes with diameter of 16 mm was sealed with a rubber stopper; the paraffin RT 31 was warmed until it completely melted and the molten paraffin was poured into a stainless steel tube.

To maintain the homogeneity of the samples, the tube was also heated until all of the paraffin in the tube was in the liquid state. The tube was cooled at a room temperature. When paraffin was solidified in the tube, the rubber stopper was replaced with a plastic cylinder. By pushing in a plastic cylinder to the tube, at different ends of the tube a paraffin cylinder was extruded and cut on different thicknesses. The resulting paraffin tablet was inserted between two flat glass pieces, which were first washed in acetone and placed for 10 min in an ultrasonic bath. An extrusion tube and samples of various thicknesses are shown in Fig. 2.

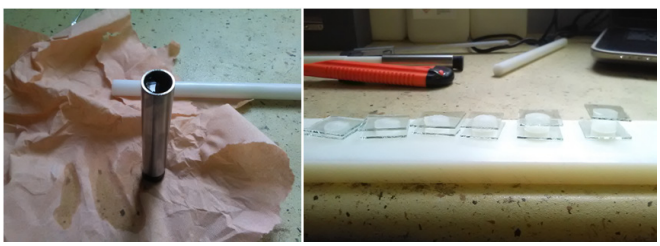

Fig. 2. Extruder with samples of various thicknesses.

Spectrophotometer Specord 210 was used to measure the total transmittance of paraffin. The total transmittance was measured by an integral sphere, in the wavelength range from 200 to 1100 nm.

4. RESULTS AND DISCUSSION

4.1. Total Transmittance Measurements for Different Thicknesses of RT35 Paraffin

Figure 3 shows the total transmittance spectra of various thicknesses of PCM in the light wave range from 400 to 1100 nm. It can be seen that transmittance of a single thickness sample in this light range is flat and a slight absorption peak appears at 940 nm [4]. As thickness of the sample increases, transmittance decreases and, accordingly, absorption increases, which was expected from the Buger-Lambert law [5].

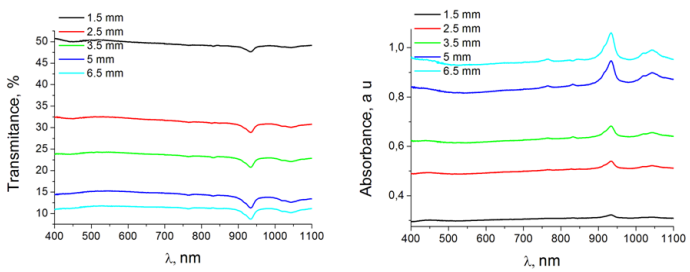

Fig. 3. Total transmittance and absorption spectra for different thicknesses of RT35 paraffin.

Dependence of paraffin thickness and average absorption is shown in Fig. 4. In order to obtain a functional relationship between sample thickness and absorption, a regression equation was generated for the graph of Fig. 4. The following logarithmic relation was obtained:

$$A = 0.448\mathbf{9}\,(d) + 0.104\mathbf{6}, \tag{2}$$

where d – sample thickness and A – absorbance of sample.

The correlation coefficient R2 of the regression equation obtained was 0.9917, indicating a strong correlation.

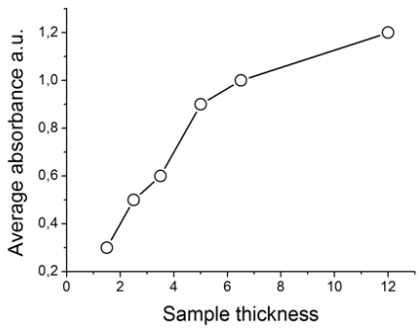

Fig. 4. Dependence of paraffin RT35 thickness and absorption.

By introducing hypothesis (1) of this paper in equation (2), it is possible to obtain a functional correlation between the absorption of the paraffin layer with thickness h at different angles of incidence α:

$$A = 0.448\mathbf{9}\left(\frac{h}{cos\alpha}\right) + 0.104\mathbf{6}. \tag{3}$$

4.2. Dependence of Glass Absorption on the Angle of Light Incidence

Absorption spectra were taken for a 2 mm glass sample at four different angles: 10, 20, 30 and 40 degrees in the light wave range from 400 to 1100 nm. The average absorption values obtained at four angles are shown in Fig. 5. It is seen that the absorption values exponentially increase. Compared to the absorption of paraffin, the absorption of glass is more than ten times smaller. However, at higher angles of incidence, this is significant and should be included in the model. For this purpose, in Fig. 5 the empirical curve was subjected to the regression analysis and the regression equation was generated (Fig. 5, the red curve):

$$A = 0.095 + 0.0023e^{\alpha 0.069}, \tag{4}$$

where A – glass sample absorption and α – light angle of incidence.

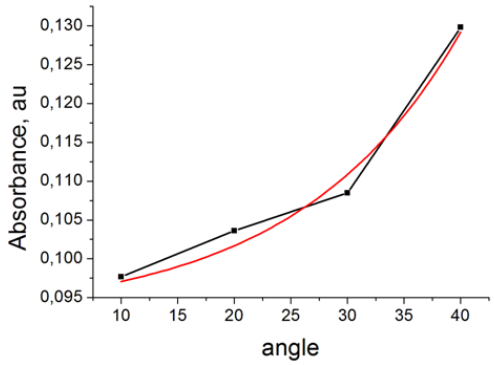

Fig. 5. Absorption of the glass sample at different angles of incidence.

4.3. Total Absorbance and Total Transmittance of Glass and Paraffin

Knowing the dependence between the absorption of paraffin and on the angle incidence and absorption of glass from the angle of incidence, the total absorption can be obtained by summing up the individual absorbance expressed in equations (3) and (4):

$$A_{total} = 0.4489\,\mathrm{h}\left(\frac{h}{\cos\alpha}\right) + 0.0023e^{0.069\alpha} + 0.1996\,. \tag{5}$$

Knowing absorption, it is necessary to calculate transmittance. Due to the fact that the absorption coefficient here is quite generalized, we first experimentally found the absorption and transmittance dependence, obtaining an empirical equation. A graph demonstrating the dependence between absorption and transmittance is presented in Fig. 6.

The regression equation is as follows:

$$T = 99.864e^{-2.29\cdot A_{total}}. \tag{6}$$

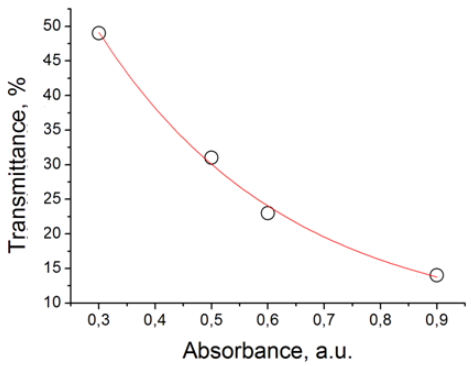

Fig. 6. Dependence between absorption and transmittance (determined experimentally as an empirical relation).

It can be seen that the dependence shown in Fig. 6 is functional with a correlation coefficient – 1 (one). This equation is used by the apparatus to calculate transmittance from absorption data. We will also use this dependence to calculate the total absorbance transmittance.

Using equations (5) and (6), it is possible to obtain the total transmittance dependence on the angle of incidence of light and the paraffin layer thickness in the common system glass-paraffin-glass:

$$T_{total} = \mathbf{9}\ .864e^{-2.299 A_{Total}} = \\ = \mathbf{9}\ .864e^{-2.299\left(0.4489\,\mathrm{h}\left(\frac{h}{\cos\alpha}\right)+0.0023e^{0.069\alpha}+0.1996\right)}. \quad (7)$$

To visualise the total transmittance dependence on the angle of incidence of light, transmittance was calculated according to equation (7) for a 12 mm paraffin layer, coated on both sides with 2 mm glass. The obtained data are graphically shown in Fig. 7.

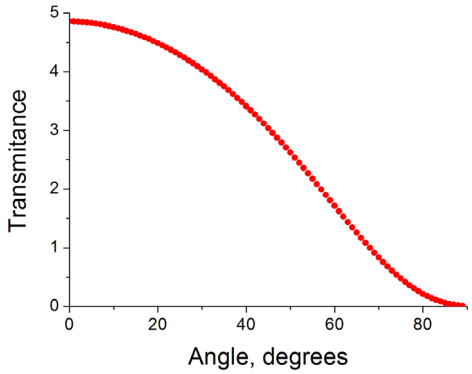

Fig. 7. The dependence of transmittance on the common system of the incident light angle, which on both sides is 4 mm glass and in the middle is 12 mm of the RT31 paraffin.

5. CONCLUSIONS

Theoretical models conclude that light beam shines on the PCM layer at different angles horizontally and vertically because of different sun position.

The theoretical models conclude that the luminance of the luminance through the PCM layer varies horizontally and vertically from different angles, as the sun positions differ.

According to a conventional window form, light beam goes through a thicker layer of PCM in case of perpendicular beam direction. Pure paraffin is homogeneous in the liquid phase and the solid phase of paraffin has small crystals with directorial structure. Crystal form has insignificant impact on results in case with big size samples. Hence, light reflection and absorption depend on PCM thickness and angles of incidence of the rays.

Experimental results show that according to the theory, transmittance of a single thickness sample in this light range is straight and a slight absorption peak

appears at 940 nm. Regression equation has been generated for determination of dependence of the tested paraffin thickness and absorption. Dependence of glass absorption on the angle of light incidence has been determined. Moreover, the total transmittance dependence on the angle of incidence of light and the paraffin layer thickness in the common system glass-paraffin-glass has been obtained.

REFERENCES

1. World Energy Council. (2013). *World Energy Perspective.* UK: World Energy Council. ISBN: 978 0 94612 126 7.
2. Socaciu, L. G. (2012). Thermal energy storage with phase change material. *Leonardo Electronic Journal of Practices and Technologies*, *20*, 75–98. ISSN 1583-1078.
3. Ismail, K. A. R., Salinas, C. T., & Henriquez, J. R. (2008). Comparison between PCM filled glass windows and absorbing gas filled windows. *Energy and Buildings 40*, 710–719.
4. Fokaides, P.A., Kylili, A., & Kalogirou, S. A. (2015). Phase change materials (PCMs) integrated into transparent building elements: A review. *Materials for Renewable and Sustainable Energy, 4*(2), Article 6. DOI 10.1007/s40243-015-0047-8.
5. GlassX North America. (2018). *GlassX's website, Home*. Available at *http://www.glassxpcm.com*
6. Ismail, K. A. R., & Henriquez, J. R. (2001). Thermally effective windows with moving phase change materials curtains. *Applied Thermal Engineering, 21*, 1909– 1923.
7. Rubitherm. (2018). *Rubiherm's website, RUBITHERM® PCM's*. Available at *http://www.rubitherm.de/english/*
8. Swinehart, D. F. (1962). The Beer-Lambert law. *Journal of Chemical Education*, *39*(7): 333. DOI: 10.1021/ed039p333.

JAUNĀ TIPA STIKLOJUMA OPTISKĀS ĪPAŠĪBAS, KAS MODIFICĒTAS AR FĀZMAIŅAS MATERIĀLU (TEORĒTISKĀ PIEEJA)

M.Vanags, K.Ļebedeva, A.Snegirjovs, G.Kaškarova, P.Šipkovs

K o p s a v i l k u m s

Publikācija iepazīstina ar fāzes maiņu materiālu (FMM) izmantošanu ēkas logos, kas tika pētīta ERA-NET-LAC projekta "Saules hibrīda caurspīdīgs elements siltuma enerģijas uzglabāšanai ēkās" ietvaros. Galvenais mērķis šajā pētījumā ir ēku energotaupības palielināšana. Lai sasniegtu uzdevuma mērķus, tika nolemts izveidot teorētisku modeli FMM ietekmei uz loga īpašībām un pēc tam eksperimentāli pārbaudīt modeli. Kā vispiemērotākais un pieejamais FMM tika izvēlēts parafīns. Tīram parafīnam ir augsta caurspīdība šķidrā fāzē un blāvi balta krāsa cietā fāzē. Publikācijā parādīti kopējās caurlaidības un absorbcijas spektru rezultāti dažādiem parafīna biezumiem ar kušanas temperatūru 35°C, kā arī parādīts stikla parauga absorbcija ar FMM dažādos gaismas krišanas leņķos.

17.12.2018.

sciendo

LATVIAN JOURNAL OF PHYSICS
AND TECHNICAL SCIENCES
2019, N 1

DOI: 10.2478/lpts-2019-0003

STUDY OF THE PROCESSES OF NEAR IDENTICAL, NANOPRENE, NEURO PROGENITOR ELECTRIC DRIVE

Viktor M. Buyankin
Bauman Moscow State Technical University, 2-nd Baumanskaya Str. 5, 105005, Moscow, RUSSIA
Viktor-Buyankin@yandex.ru

The article deals with the artificial multilayer neural network with direct signal transmission and reverse error propagation, which operates in the mode of identification of static and dynamic characteristics of the electric drive. To study processes of nearly identical, nanoprene of neuroprogenitor has been developed by the research stand, which is described in the article. As a result of research on the stand, the results show that the neural network is well enough to identify the static and dynamic characteristics of the electric drive.

Keywords: *clustering, drive, materials science, neural network, training*

1. INTRODUCTION

Neural networks are used in industrial units in the presence of disturbing effects on the control object when traditional solutions in control systems are not effective enough [1]–[4]. Management of electric drive complexes, using neural networks, is advisable when changing in a wide range of parameters of the mechanical part and modes of operation of the electric drive when the speed or accuracy of traditional control systems with linear regulators is insufficient [5].

The neural network is able to perform a variety of functions: managing dynamic objects, hardware diagnostics, forecasting, production management, monitoring of technological processes [6]. When using neural networks, it is possible to carry out parallel processing of information by all links, which significantly accelerates the processing of information [7]. Neural networks are characterised by the ability to learn and summarise accumulated knowledge [8]– [11]. The network trained on a limited set of data is capable of further generalising the received information and processing the data which were not used at its training [12].

Multilayer neural network performs the function of an adaptive object controller in the dynamic control system. In this case, the neural network in the learning process simultaneously forms the optimal control effect on the input of the system actuator in the sense of minimality of the required target function [13]. The goal of learning the network and the goal of managing the object are the same,

which means setting a common target function [14]. There is a possibility when the network operation consists of two stages: the stage of training the network optimal control law, calculated in advance on the basis of any theory in accordance with the specified training functionality; and the stage of reproduction of the optimal control function at the outlet of the network or at the entrance of the actuator. Here the target functions of network learning and object management can differ from each other. The latest version of the multi-layer neural network for management has been found to be predominant for a number of reasons [15].

2. METHODS

A multilayer neural network is used as the state IDs of the nonlinear dynamic objects, successfully competing with traditional linear and nonlinear identities. It should also be noted that a multilayer neural network is used as an optimizer for tuning traditional adaptive regulators [16]. The network is fully defined if its architecture, i.e., the method of connection of basic elements is specified, and the algorithm of its training is adopted in accordance with the method of training [17]. Neural networks allow creating a model of the object that accurately conveys its dynamics, while not requiring additional knowledge about the structure and parameters of the object [18]. Only the input and output signal values are the necessary data, so the object is represented as a black box.

Neural networks are used in industrial units in the presence of disturbing effects on the control object when traditional solutions in control systems are not effective enough. Management of electric drive complexes, using neural networks is advisable when changing in a wide range of parameters of the mechanical part and modes of operation of the electric drive when the speed or accuracy of traditional control systems with linear regulators is insufficient.

3. RESULTS AND DISCUSSION

The most common architectures of neural networks are direct distribution networks, recurrent neural networks, self-organizing maps or Kohonen network, convolutional neural networks, and radial basis functions. The number of neural network architectures is tens, and for different types of tasks, different types of neural networks are most effective. Neural networks allow creating a model of the object that accurately conveys its dynamics, while not requiring additional knowledge about the structure and parameters of the object. Only the input and output signal values are the necessary data, so the object is represented as a black box. Let us consider management with predictive models [5], [19], [20]. The controller uses a neural network model of a nonlinear object to predict the behaviour of the control object on different types of input actions. Building an object model is called system identification. The process of constructing a neural network model of an object consists of the following steps: 1) data collection and normalization for training; 2) choice of network architecture and learning algorithm; 3) training; 4) checking the adequacy of training.

The constructed object model is used to create a control system for this object. The task of the neurocontroller is to calculate the control signal that will optimise the operation of the object for a certain period of time. A prediction error between the output of a control object and the output of its neural network model is used as a signal to train the network.

Neural networks and neuro-controllers can be used to control various objects, including electric drives of various mechanisms, while the neuro-controller produces a control signal. The neural network on the first iterations of the learning process can give control signal values that are not valid, for example, for an electric drive. Therefore, the configuration of the neurocontroller should be done using the object model.

To study processes of near identical, nanoprene of neuroprogenitor was developed by the research stand sketch, which is shown in Fig. 1. The basis of the stand design is standard laboratory table 1. A panel with sockets is mounted vertically on the table to measure the required parameters of various units of the electric drive control system. This panel is assigned a blank panel with 2 done on it mnemonic in the block diagram of the actuator, which is shown in Fig. 1, where inappropriate places, the indication of the rotation angle and speed of the drive shaft by means of LEDs and seven-segment elements are displayed. DC motor (3), load device (4) and a pulse sensor (5) are mounted on special vertical (to save space) frame – a rack mounted on the floor to the right of the bench of the Microcomputer unit of the programming device (7) and the power source load device (8) located on the lid of the instrument tables (9), which is mounted to the left of the stand with the engine. In the Cabinet (9), crate (10) is mounted with the electronic components of the control system. In the crate, there is also the necessary functional switching equipment. Such arrangement and constructive execution of block (10) give the chance of free access to printed circuit boards of electronic blocks in case of their study or repair. The proposed location of the equipment, a corresponding functional block diagram (Fig. 1) of electric drive systems, ensures efficient and safe operation with the bench.

Figure 1 presents a drive with a PBST-22 DC motor, which has the following nominal parameters: P = 0.6 kW, U = 110 V, I = 7 A, n = 1000 vol. The circuits of negative feedback are closed through a microcomputer using a pulse sensor, from which you can get information about the speed and angle of rotation of the motor shaft. The functional scheme of the electric drive consists of micro-computers, programmer, interface, code-phase converter, pulse distributor, power unit, DC motor, Tacho, pulse sensor unit angle code with digital indication of the angle of rotation and the speed of the motor shaft. To study and measure the mechanical characteristics of the stand, a load device is provided. The enlarged algorithm of operation of the electric drive can be represented as follows: electric drive with DC motor is made on the principle of a non-autonomous digital automated control system, in which a comparison of the master and the workable codes takes place directly in the micro-computer.

The control signal from the micro-computer is given to the converter code phase and then through the power unit is fed to the executive DC motor. Misalignment error between the driver and the feedback is worked out in the digital correcting device of the microcomputer. Micro-computer has a modular principle of

construction, i.e., all functional blocks are made in the form of structurally complete devices (modules), communication between which is carried out through a single channel of information exchange. Thus, a microcomputer is a system of modules united by a channel. Parallel exchange links connect the CPU, memory, and all external devices. All modules are connected to the channels of the micro-computer. Communication through the channels is closed, i.e., the control signal supplied by the active device must receive a signal from the passive device.

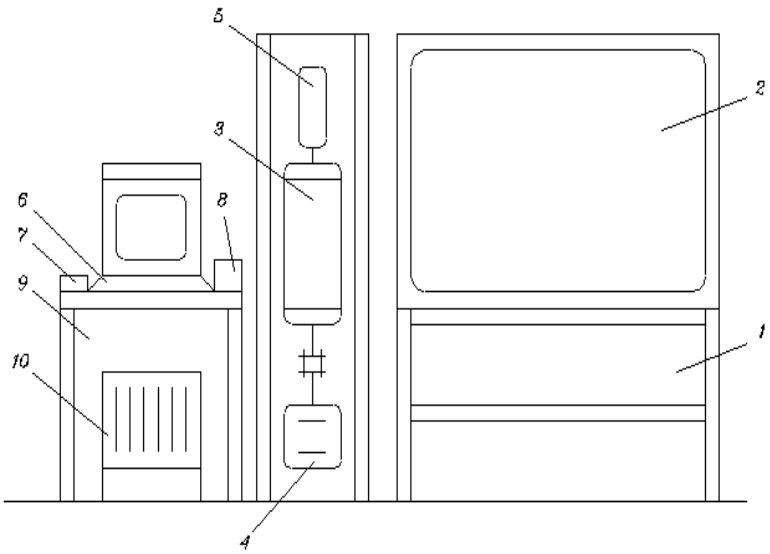

Fig. 1. Stand of the drive for research of near identical, nanoprene, neuroprogenitor: 1 – programmer, 2 – traffic, 3 – controller, 4 programs of name identifier, nanoprene, propagation, 5 – timer, 6 – UI, 7 – power unit, 8 – transducer angle code, 9 – in a network: 10 – current sensor, 11 – motor, 12 – speed sensor 13 – sensor of the rotation angle.

The main element of the microcomputer is the central processor, which controls the distribution of the time of use of the channel by external devices and performs all the necessary arithmetic and logical operations for processing information. It contains 16 general-purpose high-speed registers, which are widely used in various operations. At the same time, the CPU performs several operations, the team extended arithmetic can be treated as sixteen-bit or 8-bit words.

The ability to use eight addressing methods allows for highly efficient processing of data stored in any memory cell or register. The operating unit performs the operations of generating addresses of commands and operands, logical and arithmetic, storing operands and results. The firmware control unit produces a sequence of micro-commands based on the received command code. It encodes a complete set of micro-commands for all types of commands. The interrupt block organises a priority interrupt system, performs reception and pre-processing of internal and external interrupt requests of the computational process.

The interface unit performs the exchange of information among devices located on the system highway, performs arbitration during operations, direct

memory access. A sequence of control signals of the system trunk is formed in the interface block. The block system of highways connects the inner pipe with the outer. It manages amplifiers receiving and issuing information on the combined conclusions of addresses and data.

The functional scheme of the electric drive, which represents the three-circuit digital tracking system of automatic regulation, is presented in Fig. 2. The contours of the negative OS are closed with the help of current sensors, speed, and angle of the shaft of the motor through a microcomputer.

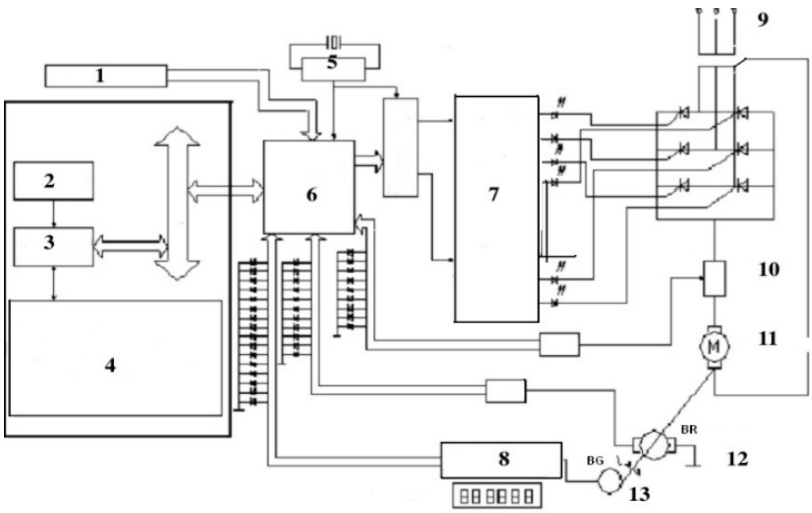

Fig. 2. A functional diagram of the electric drive: 1 – programmer, 2 – traffic, 3 – controller, 4 programs of name identifier, nanoprene, propagation, 5 – timer, 6 – UI, 7 – power unit, 8 – transducer angle code, 9 – in network: 10 – current sensor, 11 – motor, 12 – speed sensor, 13 – sensor of the rotation angle.

The actuator consists of a macro-computer, interface, converter "code-phase" of distributor pulses, a block of the thyristor, DC motor, Tacho-generator, current sensors, speed and angle of the shaft of the motor, the two ADC converter "angle-code", timer, programmer and load of the device. The microcomputer performs the function of processing the signals from the sensors to the OS that carries out the preset movement program. Adaptive reconfigurable controller, which is implemented in software, provides optimum operation. The channel of communication with external devices in microcomputers is a common bus. The interface provides communication with external devices, microcomputers, delirium addresses of the sensors OS and generates return service signals. The decoded signals of the respective bits are used as address signals of the blocks of the drive. The interface has two channels for transmission from the microcomputer to the external device and receiving data from external devices. Command INPUT or OUTPUT to the bus channel of the microcomputer connects certain external devices.

The angle-code converter measures the rotation angle of the motor shaft in a parallel binary code with fifteen digits. Upon request, personalized information is sent to a receiver channel interface. Converter "code-phase" converts the parallel

binary code at the output of the microcomputer in the control pulses, a phase shift which is directly proportional to the binary code. Distributors of pulses in sequence provide the control electrodes of the thyristor VDI...VD6 control pulses. The timer, which is based on a quartz oscillator, provides a highly stable frequency of time signals for synchronizing the operation of all nodes of the functional circuit of the electric drive. ADC is used to convert analogue signals from the current sensor and Tacho-generator in a parallel binary code and transmit these signals to microcomputer.

The thyristor unit consists of thyristors and a three-phase transformer, whose secondary windings are connected to a three-phase star with a zero output. The transformer matches the mains voltage with the motor supply voltage and limits short-circuit currents. The motor is connected at one end to the zero output of the secondary windings of the transformer, and the other – to the inverter and rectifier groups of thyristors. The current sensor is a measuring device of the resistive type.

Tacho is an element of automatic control systems, the input parameter for which is the rotational speed (angular position) of the Tacho shaft, and the output – the voltage directly proportional to the input value. Pulse type feedback sensor includes three main parts: mechanical, optical and electronic. These signals have a rectangular shape, their amplitudes are shifted relative to each other by 90°. Pulse repetition rate is proportional to the measured rotational speed, and the number of pulses – the angle of rotation of the motor shaft.

To display information about the rotation angle and speed of the motor shaft, a digital display is provided on the stand. The rotation angle is displayed using the seven-segment indicator made on the LEDs, which receives signals from the decoder that translates the binary code into the control code of the seven-segment indicators. The load device, consisting of an autotransformer T2, voltmeter PV, ammeter RA and powder coupling, is used to create the load moment on the motor shaft, which is directly proportional to the current flowing in the powder coupling circuit.

The laboratory setup consists of a microcomputer, which is administered by the keyboard of the programming device and the power unit mounted on the supporting metal structures. Electronic function blocks are located in a special device (under the computer). Beside the computer there is a stand, which shows a functional diagram of the actuator for the study of processes of near identical, nanoprene, neuroprogenitor physical processes in DC motors.

The motor speed at low frequencies is unstable and the coefficient of unevenness increases with a decrease in the speed. This is understandable, since with the decrease in the motor speed, the nonlinearity of the type of dry and viscous friction in the bearings of the motor, the nonlinearity of the type of magnetic saturation in the stator and rotor cores, additional losses due to the dispersion of the electromagnetic field created by the excitation winding begin to affect more and more.

To identify static and dynamic characteristics, it is necessary to use a neural network containing 20 neurons with tansig activation function in the first input layer and 1 neuron in the output with purelin activation function, which is described by the system of equations:

$$Y_1 = Y_0 Z^{-1}. Y_2 = Y_0 Z^{-2}. Y_3 = Y_0 Z^{-3} \quad (1)$$

The output signals of the neural network were detained in 1, 2, 3 tact. Equations of the 1st output layers of neurons:

$$\left.\begin{aligned} E_1 &= X_0 W_1 + Y_0 W_2 + Y_1 W_3 + Y_2 W_4 + Y_3 W_5 + B_1 \\ E_2 &= X_0 W_2 + Y_0 W_2 + Y_1 W_3 + Y_2 W_3 + Y_3 W_3 + B_2 \\ &\ldots\ldots\ldots\ldots\ldots\ldots\ldots\ldots\ldots\ldots\ldots\ldots\ldots\ldots\ldots\ldots\ldots\ldots\ldots\ldots \\ E_2 &= X_0 W_{211} + Y_0 W_{212} + Y_1 W_{213} + Y_2 W_{214} + Y_3 W_{215} + B_2 \end{aligned}\right\} \quad (2)$$

Equations of the 2nd output layer of neurons:

$$\left.\begin{aligned} R_1 &= \tan sig(E_1) \\ &\ldots\ldots\ldots\ldots\ldots \\ R_2 &= \tan sig(E_2) \\ Y_0' &= R_1 W_1' + \ldots\ldots\ldots\ldots + R_2 W_2' + B_1' \\ Y_0 &= pureline Y_0' \end{aligned}\right\} \quad (3)$$

Figures 3-4 demonstrate structural diagrams of the neural network.

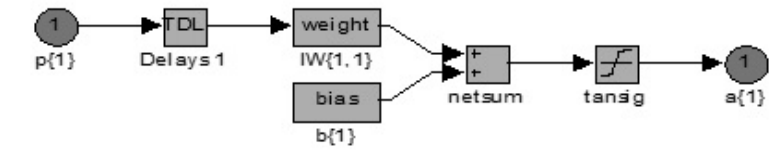

(a)

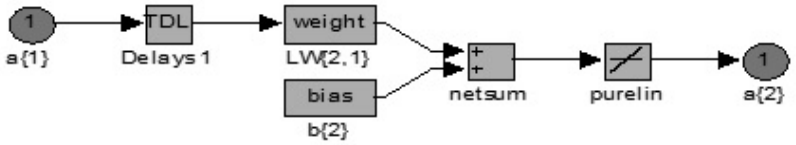

(b)

Fig. 3. The structural diagram of neural network: (a) first layer, (b) second layer.

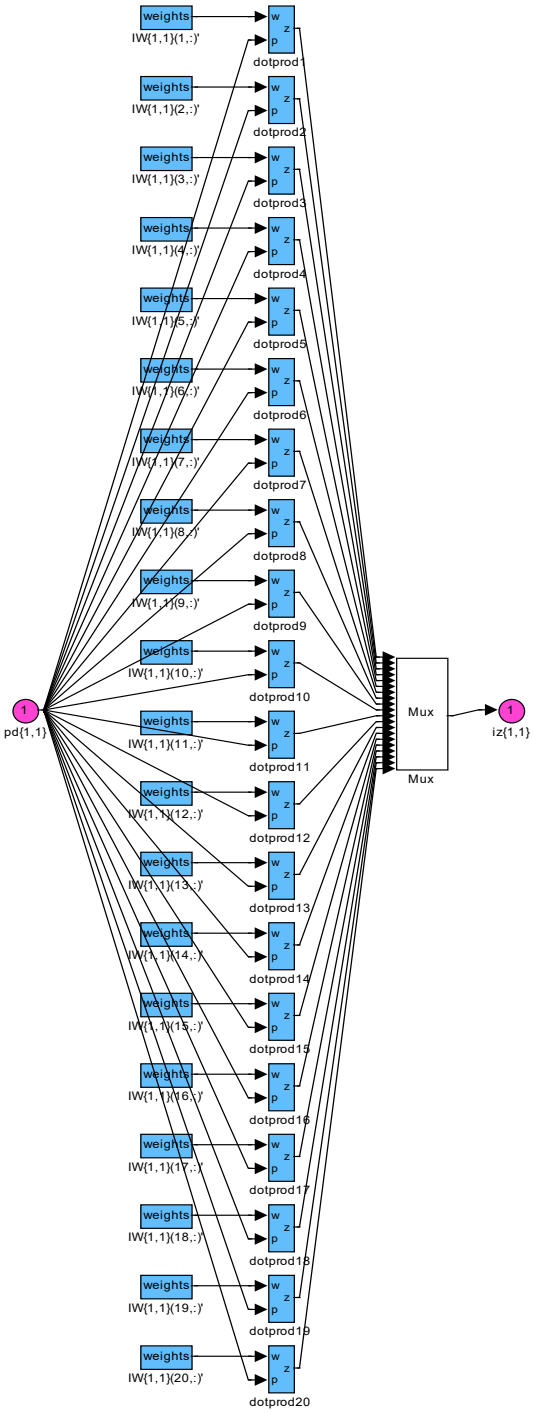

Fig.4. A detailed diagram of the neural network.

The results of near identical static and dynamic characteristics of the actuator are shown in Figs. 5, 6, 7.

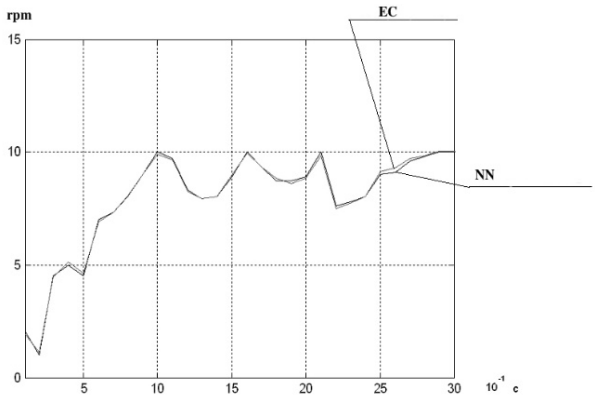

Fig. 5. Near identical operation at a preset speed 9 rpm: ED – electric drive, NN – neural network.

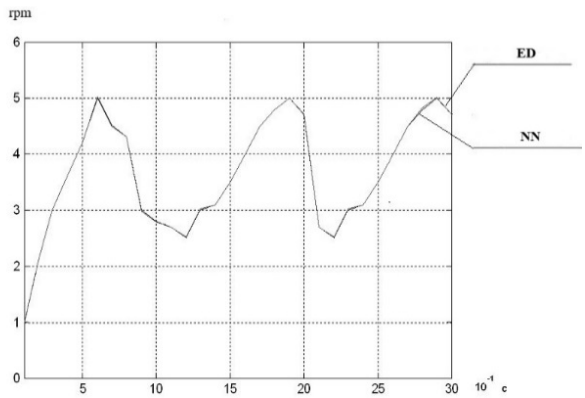

Fig. 6. Near identical operation at a preset speed 4 rpm: ED – electric drive, NN – neural network.

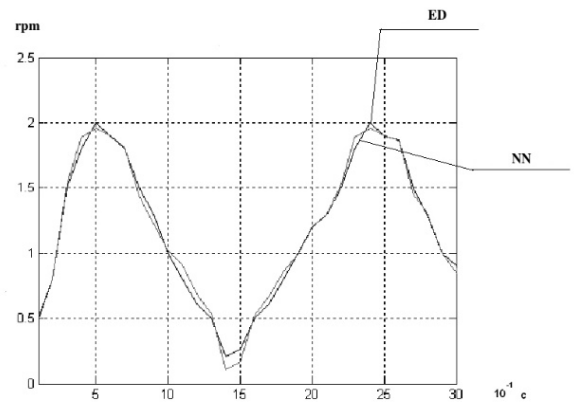

Fig. 7. Near identical operation at a preset speed of 1 rpm: ED – electric drive, NN – neural network.

Thus, as a result of experimental studies on the stand, the results were obtained, which showed that the neural network could accurately identify the static and dynamic characteristics of the electric drive.

4. CONCLUSIONS

From the presented graphs, it can be seen that the neural network copes with the task of identification, with high accuracy repeating the dynamics of the model of the electric drive in the entire range of its operation. This method can be applied to electric drives of any complexity. The disadvantage of the method is the need for learning the model to test its adequacy with new data that did not participate in the training. This is due to the danger of re-training the network. This problem can be solved by programmatically controlling the learning outcome before application. Thus, the use of neural networks as an alternative to existing algorithms for identification and construction of linear multidimensional mathematical systems is quite possible.

An expert system of forecasting the technical condition of the product on the basis of the mathematical apparatus of artificial neural networks (ins) has been proposed. Hybrid artificial neural networks are a combination of different kinds of neural networks and concepts of their training. They are designed to solve various kinds of problems, such as pattern recognition, prediction, approximation of functions, etc.

The problem of forecasting the technical condition of the product on the basis of the mathematical apparatus of artificial neural networks is formalized through the problem of pattern recognition. The data on the predicted variable for a certain period of time form an image, the class of which is determined by the value of the predicted variable at some point outside of this interval, i.e., the value of the variable through the prediction interval.

REFERENCES

1. Fard Masoumi, H.R., Basri, M., Kassim, A., Kuang Abdullah, D., Abdollahi, Y., & Abd Gani, S.S. (2014). Comparison of estimation capabilities of the artificial neural network with the wavelet neural network in lipase-catalyzed synthesis of triethanolamine-based esterquats cationic surfactant. *J Surfactants Deterg*., *17*(2), 287–294. doi: 10.1007/s11743-013-1539-0.
2. Mao, W., Wang, W., Dou, Z., & Li, Y. (2018). Correction to: Fire recognition based on multi-channel convolutional neural network. *Fire Technol*. doi: 10.1007/s10694-018-0705-3.
3. Ayhan, T., Karlik, B., & Tandiroglu, A. (2008). Flow geometry optimization of channels with baffles using neural network and second law of thermodynamics. *Comput Mech*., *42*(3), 481. doi: 10.1007/s00466-006-0083-4.
4. Yamada, T. (2009). Remarks on the tracking method of neural network weight change for a learning-type neural network feed-forward feed-back controller. *Artif Life Robot*., *14*(3), 384. doi:10.1007/s10015-009-0690-1.
5. Buyankin, V.M., Vasiliev, V.V., Tikhomirov, E.L., & Tochilina, N.S. (1983). Drive control in microprocessor systems. In *Microprocessor Technology in CNC Machine Tools*: *Sat. Scientific Papers* (pp. 43–51). Moscow: ENIMS.
6. Posyagin, A.I., & Yuzhakov, A.A. (2013). Development of a two-layer neural network for a self-routing analog-to-digital converter based on a neural network. *Russ Electr Eng*., *84*(11), 602–605. doi: 10.3103/S1068371213110114.

7. Lin, H-L., Chou, T., & Chou, C-P. (2007). Optimization of resistance spot welding process using taguchi method and a neural network. *Exp Tech*., *31*(5), 30–36. doi:10.1111/j.1747-1567.2007.00186.x.
8. Virili, F., & Freisleben, B. (2001). Neural network model selection for financial time series prediction. *Comput Stat*., *16*(3), 451–463. doi: 10.1007/s001800100078.
9. Liu, P., Shi, R., & Gao, W. (2018). Erratum to: Estimating leaf chlorophyll contents by combining multiple spectral indices with an artificial neural network. *Earth Sci Informatics*, *11*(1), 157. doi: 10.1007/s12145-017-0325-3.
10. Alkhasawneh, M.S., & Tay, L.T. (2017). A hybrid intelligent system integrating the cascade forward neural network with elman neural network. *Arab J Sci Eng*. doi: 10.1007/s13369-017-2833-3.
11. Wang, H., Lv, Y., Chen, H., Li, Y., Zhang, Y., & Lu, Z. (2018). Erratum to: Smart pathological brain detection system by predator-prey particle swarm optimization and single-hidden layer neural-network. *Multimed Tools Appl*., *77*(3), 3887, doi: 10.1007/s11042-017-4391-9.
12. Patra, J.C., Ang, E.L., Chaudhari, N.S., & Das, A. (2005). Neural-network-based smart sensor framework operating in a harsh environment. *EURASIP J Adv Signal Process*, *2005*(4), 498294. doi:10.1155/ASP.2005.558.
13. Shaltaf, S. (2004). Neural-network-based time-delay estimation. *EURASIP J Adv Signal Process*, *2004*(3), 654087. doi: 10.1155/S1110865704309261.
14. Nemmour, H., & Chibani, Y. (2005). Neural network combination by fuzzy integral for robust change detection in remotely sensed imagery. *EURASIP J Adv Signal Process*, *2005*(14), 413784, doi:10.1155/ASP.2005.2187.
15. Dmitriev, A.S., Emelyanov, R.Y., Lazarev, V.A., & Chibisov, V.V. (2017). Simulation of dynamics of the neural ensemble in an active wireless network. *J Commun Technol Electron*, *62*(10), 1148–1151. doi: 10.1134/S1064226917100035.
16. Hartmann, C., Lazar, A., & Triesch, J. (2015). Key features of neural variability emerge from self-organized sequence learning in a deterministic neural network. *BMC Neurosci*., *16*(1), 266. doi: 10.1186/1471-2202-16-S1-P266.
17. Nugent, C.D., Lopez, J.A., Smith, A.E., & Black, N.D. (2002). Prediction models in the design of neural network based ECG classifiers: A neural network and genetic programming approach. *BMC Med Inform Decis Mak*., *2*(1), 1. doi: 10.1186/1472-6947-2-1.
18. Rohit, S., & Chakravarthy, S. (2011). A convolutional neural network model of the neural responses of inferotemporal cortex to complex visual objects. *BMC Neurosci*., *12*(1), 35. doi: 10.1186/1471-2202-12-S1-P35.
19. Grasel, F.D.S., & Fontoura, L.A.M. (2016). Computacional study of the electronic effects in rotational barrier of the N-arilcarbamatos N-CO bond. *Periodico Tche Quimica*, *13*(25), 7–15.
20. Buyankin, V.M., & Vasiliev, V.V. (1982). Digital servo drive with separate control reversing thyristor Converter. In *Electric and Hydraulic Drive of CNC Machines and Industrial Robots*: *Sat. Scientific Papers* (pp. 78–86). Moscow: ENIMS.

GANDRĪZ IDENTISKAS, NANOPRĒNA, NEIRO-PROGENERATORA ELEKTRISKĀS PIEDZIŅAS PROCESA PĒTĪJUMS

V. M. Bujankins

K o p s a v i l k u m s

Rakstā aplūkots mākslīgs daudzslāņu neironu tīkls ar tiešu signālu pārraidi un kļūdu atgriezenisko izplatīšanu, kas darbojas elektriskās piedziņas statisko un dinamisko īpašību identifikācijas režīmā. Lai izpētītu gandrīz identiskus procesus, pētījuma stendā, kas aprakstīts rakstā, ir izstrādāts neiro-progeneratora nanoprēns. Pētījuma rezultāti liecina, ka neironu tīkls ir pietiekami labs, lai noteiktu elektriskās piedziņas statiskās un dinamiskās īpašības.

22.12.2018.

sciendo

LATVIAN JOURNAL OF PHYSICS
AND TECHNICAL SCIENCES
2019, N 1

DOI: 10.2478/lpts-2019-0004

INVESTIGATION OF WIRELESS CHANNELS OF 802.11 STANDARD IN THE 5GHZ FREQUENCY BAND

Dmytro V. Mykhalevskiy
Department of Telecommunication Systems and Television
Vinnytsia National Technical University, 21021, 95 Khmelnytske Highway,
Vinnytsia, UKRAINE
adotq@ukr.net

The paper presents the study of wireless channel over-the-air channels of the family of 802.11x standards within the 5GHz frequency band, taking into account the influence of architectural obstacles within premises. The following parameters have been selected as the main parameters in the course of the study: an efficient rate of information transmission, signal power at the receiver input, as well as channel carrying capacity. As a result of the experimental study, the author has found out relevant mathematical expression for estimation of the efficiency criterion of wireless channels of the family of 802.11x standards for the 5GHz frequency band, taking into account relevant architectural obstacles within premises.

Keywords: *architectural obstacles, effective data rate, efficiency factor, signal strength, threshold value*

1. INTRODUCTION

Presence of quite essential quantity of devices, which require connection to the network, envisages utilisation of wireless technologies of the family of 802.11x standards because they are one of the optimum solutions for creation of the general network [1], [2].

Networks of the family of 802.11x standards are characterised by the steady development in the direction of increase of the main criterion of efficiency (efficient rate of information transmission). Taking into account the quite wide utilisation of the wireless networks, it is possible to state that a number of negative factors may appear, which can essentially worsen transfer characteristics of wireless channels of information transmission. Therefore, search of new methods and facilities for minimisation of influence of these factors is the vital task at present because such minimisation is aimed, in the first turn, at improvement of characteristics of the main quality criterion (efficient rate of information transmission).

After analysing the scientific works [3]–[11], we can conclude that it is

possible to state that wireless channels of the family of 802.11x standards are under quite strong dependence on the external destabilising factors. In this situation, quite essential fluctuations of the main criteria of efficiency occur. Therefore, the present paper will try to estimate the influence of one of the main destabilising factors (i.e., architectural obstacles) upon the main criteria of efficiency of wireless channels of the family of 802.11x standards for the 5GHz frequency band.

2. MATERIALS AND METHODS

The network was created on the basis of the access point (AP) supporting all existing standards 802.11 for the 5GHz frequency band. In addition, this AP supports the MIMO technology with three transmitting and receiving antennas (it is the most widely used equipment, which is presented on the market). For this study, the author has selected a standard premise, within which length of the wireless channel could be equal up to 15m. To estimate the influence of architectural obstacles, the author has envisaged the introduced error IE1 at the distance of $l_1=3m$, as well as the introduced error IE2 at the distance of $l_1 + l_2 = 6m$.

For this study, the following main parameter has been selected: the efficient rate of information transmission V, which is the main parameter of the criterion of the channel efficiency and which is determined by additions of the upper level of the network. In this situation, it is possible to determine the criterion of the channel efficiency as follows:

$$K = \frac{V}{V_{pl}}, \tag{1}$$

where V is the efficient rate of information transmission; V_{pl} is maximum carrying capacity of the channel, which is determined by the rate of conversion of frames into a bit sequence at the physical level and which is standardised in the specifications of the standard 802.11.

As this parameter (i.e., the rate of information transmission) is in direct dependence on characteristics of transmission of signals, the other parameter has been selected: the signal power at the receiver input P (RSSI). Estimation of the signal power has been performed through averaging the results of measurements during five minutes on the condition that the period of obtaining relevant values is equal to one second [5].

3. RESULTS AND DISCUSSION

Analysis of Results of Experimental Study

The proposed methodology was used as the basis for performance of the experimental study of the main determined parameters of wireless channels of the family of 802.11x standards in the 5GHz frequency band in order to estimate

dependence of their characteristics on certain factors of the transmission medium, such as architectural obstacles. Overall, six wireless channels were investigated. Maximum values of the parameter of carrying capacity at the physical level ($V_{pl\ max}$, MB/s) of these channels are as follows: 802.11a – 54; 802.11n, 20MHz – 216.7; 802.11n, 40MHz; 802.11ac, 20MHz – 288.9; 802.11ac, 40MHz – 600; 802.11ac, 80MHz – 1300. Variable parameter *L* is the length of the wireless channel.

The study was carried out for the following standard situations, which usually occur within the premises: open space; presence of a single door; presence of two doors; presence of one or two walls. Experimental characteristics of the channel parameters were used: a – dependence of the efficient rate of transmission on the distance between the receiver and transmitter; b – dependence of the efficient rate of transmission on the signal power at the receiver input; c – dependence of the rate of transmission at the physical level on the distance between the receiver and transmitter; d – dependence of the rate of transmission at the physical level on the signal power at the receiver input.

Open space. Open space is the most widely used scheme of construction of wireless channels of the family of 802.11x standards, when networks are created within premises. Characteristics of the channel parameters for the open space model are shown in Fig. 1.

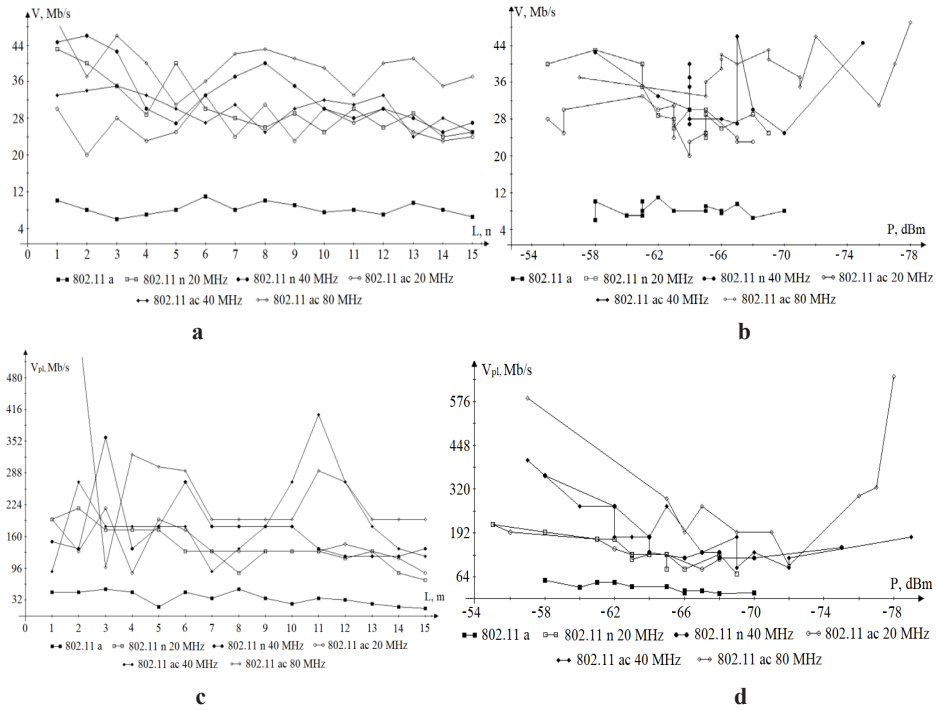

Fig. 1. Experimental characteristics of the channel parameters for the open space model.

Study results demonstrate the presence of fluctuations of the efficient rate of information transmission, which are in direct dependence of fluctuations of the signal distribution within the premises. At the same time, it is possible to estimate fluctuations of the signal for the 5GHz frequency band in accordance with the method,

which was proposed by paper [4] for 2.4GHz band. In this situation, confidence interval will vary. It is possible to write down the interval of change of fluctuations of the signal power for a general situation in the following manner:

$$P_{ñ} - \delta < P(\Delta ç\ \Delta g\ \Delta a\ \Delta b) \le P_{ñ} + \delta, \tag{2}$$

where Δc, Δg, Δa, Δb are the coefficients, which determine the limits of permissible variations of the signal attenuation coefficients; P_c is the average value of the signal power at the receiver input; δ is the coefficient of the signal fluctuations at the receiver input, which may be considered as the confidence interval.

Each confidence interval will be in correspondence with the interval of fluctuations for the selected parameter (i.e., for the rate of information transmission). Then, in respect of each standard under investigation, it would be possible to determine the relevant confidence interval for the efficient rate of information transmission ΔV, which will be in correspondence with the confidence interval of the signal fluctuations δ. Therefore, in respect of the open space channels, it is possible to write the following:

$$\delta_a \approx \pm\, 5dBm;\ \Delta V_a \approx \pm\, 2Mb/s;$$
$$\delta_{n20} \approx \pm\, 5dBm;\ \Delta V_{n20} \approx \pm\, 4Mb/s;$$
$$\delta_{n40} \approx \pm\, 5dBm;\ \Delta V_{n40} \approx \pm\, 8Mb/s;$$
$$\delta_{ac20} \approx \pm\, 5dBm;\ \Delta V_{ac20} \approx \pm\, 4Mb/s;$$
$$\delta_{ac40} \approx \pm\, 7dBm;\ \Delta V_{ac40} \approx \pm\, 8Mb/s;$$
$$\delta_{ac80} \approx \pm\, 10dBm;\ \Delta V_{ac80} \approx \pm\, 8Mb/s.$$

As it may be seen from the results obtained for the confidence intervals, an increase in the carrying capacity of a channel at the expense of the spread spectrum of this channel results in the increase of the level of fluctuations. This statement is correct both for the selected parameter and for the efficient rate of information transmission in respect of any standard. In addition, this statement is evidenced by the characteristics of the selected parameter V_{pl}, which are shown in Fig. 2c, where one may observe quite an essential dynamics of change in the values, which are determined by the MCS scheme [2].

A single obstacle – wood. This diagram simulates presence of architectural obstacles in a channel, such as wooden doors. As shown in paper [12] for 2.4GHz band, in the case of presence of a single door there is an effect of increase in the efficient rate of information transmission directly following these doors. Relevant characteristics are shown in Fig. 2. The characteristics obtained demonstrate that the signal power at the receiver input is characterised by the fluctuations, which are similar to the fluctuations that were observed in the previous situation (however, there is an exclusion).

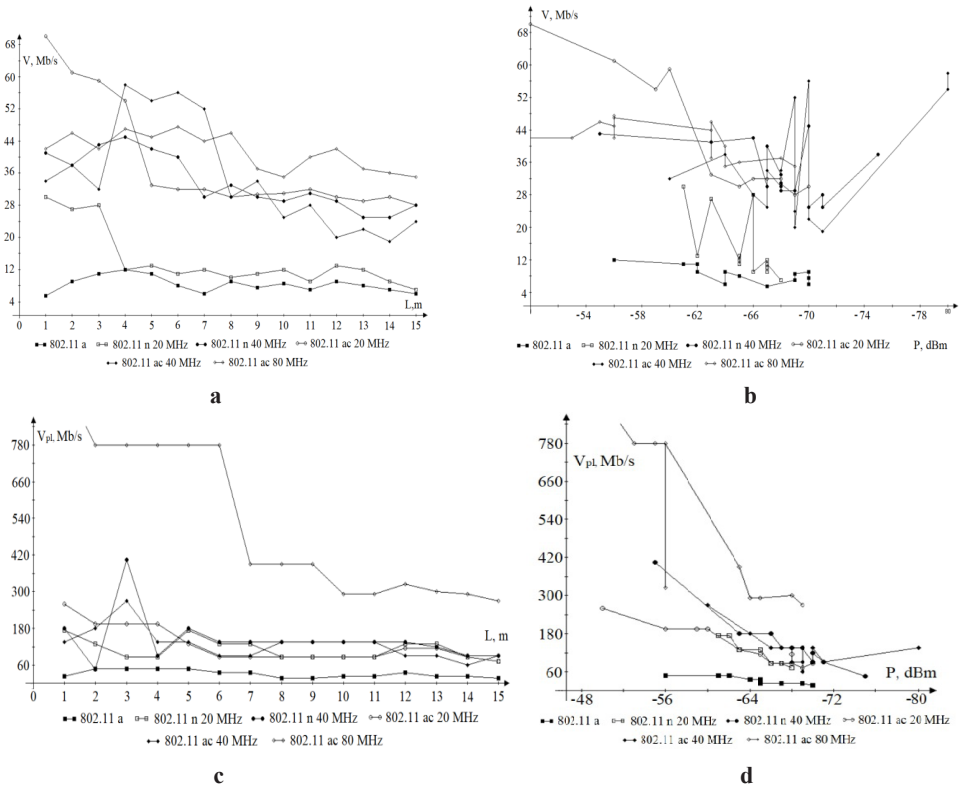

Fig. 2. Experimental characteristics of the channel parameters in the case of presence of a single obstacle.

The interval of fluctuations of the confidence interval is as follows:

$$\delta_a \approx \pm 7dBm; \Delta V_a \approx \pm 3Mb/s;$$
$$\delta_{n20} \approx \pm 6dBm; \Delta V_{n20} \approx \pm 4Mb/s;$$
$$\delta_{n40} \approx \pm 10dBm; \Delta V_{n40} \approx \pm 6Mb/s;$$
$$\delta_{ac20} \approx \pm 9dBm; \Delta V_{ac20} \approx \pm 4Mb/s;$$
$$\delta_{ac40} \approx \pm 15dBm; \Delta V_{ac40} \approx \pm 10Mb/s;$$
$$\delta_{ac80} \approx \pm 15dBm; \Delta V_{ac80} \approx \pm 10Mb/s.$$

As it may be seen from this analysis, exclusions are related to the medium of transmission near the architectural obstacle. There are quite high fluctuations of characteristics. It is possible to state that presence of a single obstacle has a minimum influence and one may neglect this influence. A single inessential increase in fluctuations is observed for the standard 802.11ac for the wideband channels, and this increase can be explained by an increase in the channel instability.

Two obstacles – wood. Such a situation is quite standard for dwelling houses and office premises. Study results are shown in Fig. 3.

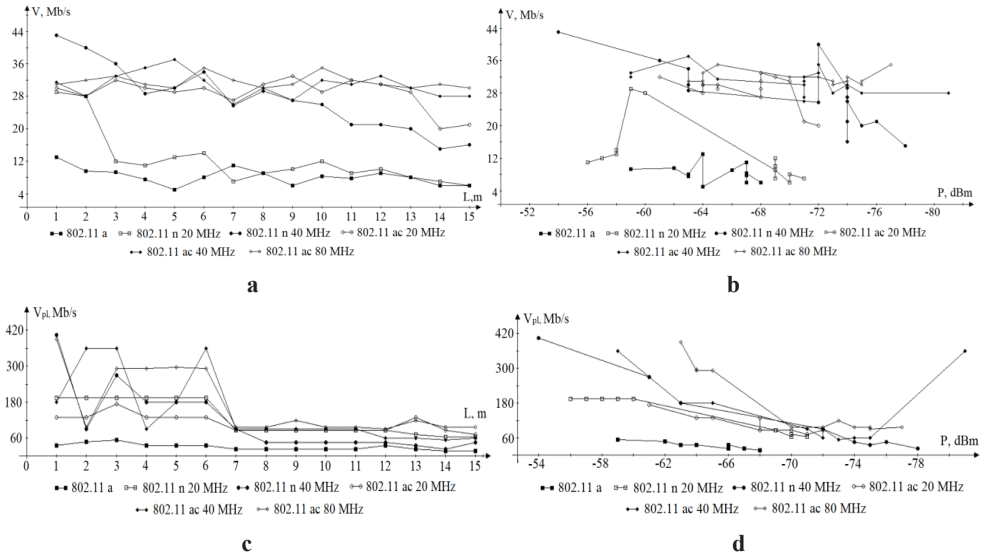

Fig. 3. Experimental characteristics of the channel parameters in the case of presence of two obstacles.

It is possible to write the fluctuations parameters of the main efficiency parameters of channels in the following manner:

$$\delta_a \approx \pm 5dBm; \Delta V_a \approx \pm 4Mb/s;$$
$$\delta_{n20} \approx \pm 6dBm; \Delta V_{n20} \approx \pm 6Mb/s;$$
$$\delta_{n40} \approx \pm 7dBm; \Delta V_{n40} \approx \pm 7Mb/s;$$
$$\delta_{ac20} \approx \pm 6dBm; \Delta V_{ac20} \approx \pm 6Mb/s;$$
$$\delta_{ac40} \approx \pm 8dBm; \Delta V_{ac40} \approx \pm 7Mb/s;$$
$$\delta_{ac80} \approx \pm 10dBm; \Delta V_{ac80} \approx \pm 7Mb/s.$$

Presence of the second obstacle made of wood in the wireless channel causes a decrease in the value of the signal power at the receiver input by 5dBm on the average. The efficient rate of information transmission is characterised by the greatest attenuation coefficient following the second obstacle. In addition, presence of the second obstacle in the wireless channel of the standard 802.11 decreases the level of fluctuations as compared with the previous situation. It follows from the charts, which are shown in Fig. 4c, that there is a certain threshold value of level of the signal power at the receiver input, below which the wireless channel begins to work in the operation mode, which is equivalent to 802.11n operation mode in the 20MHz frequency band.

Obstacles – walls. As a rule, presence of walls (as obstacles) in the wireless channel causes quite high attenuation of the signal. Study results are shown in Fig. 4.

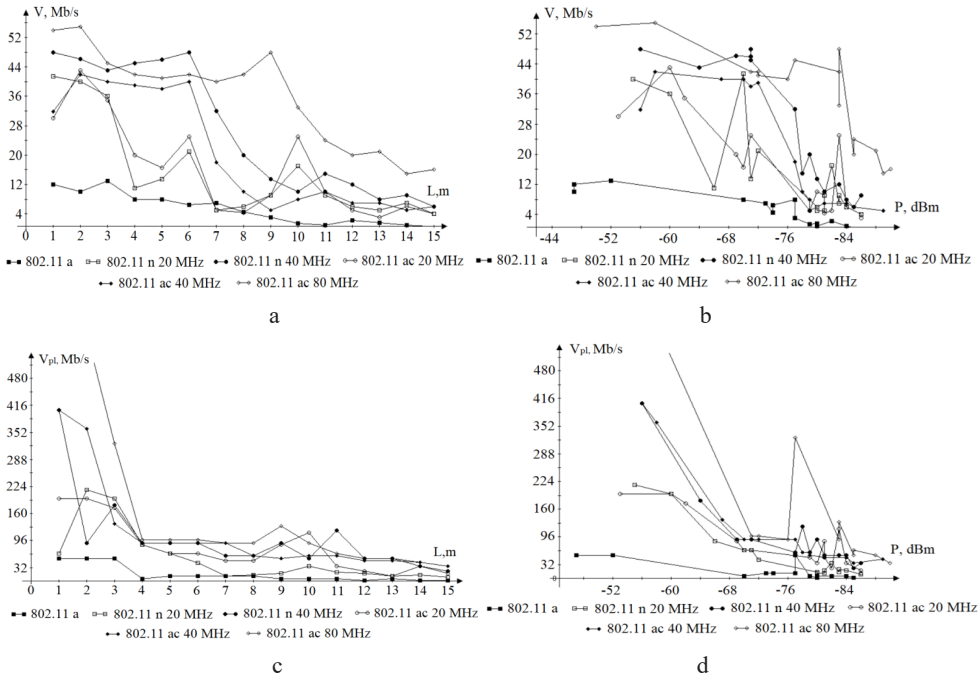

Fig. 4. Experimental characteristics of the channel parameters in the case of presence of two walls.

In this case, it is possible to observe the same restriction of carrying capacity of a channel at the physical level, and this fact confirms the assumption concerning the threshold value of the parameter of the signal power. One of the methods, which are aimed at improvement of characteristics of the efficient rate of transmission following the obstacle, is related to the use of wideband channels. Presence of the second obstacle in the channel causes an increase in the slope of attenuation of characteristics. The confidence interval for this situation is as follows:

$$\delta_a \approx \pm 15dBm; \Delta V_a \approx \pm 3Mb/s;$$
$$\delta_{n20} \approx \pm 15dBm; \Delta V_{n20} \approx \pm 4Mb/s;$$
$$\delta_{n40} \approx \pm 17dBm; \Delta V_{n40} \approx \pm 6Mb/s;$$
$$\delta_{ac20} \approx \pm 16dBm; \Delta V_{ac20} \approx \pm 4Mb/s;$$
$$\delta_{ac40} \approx \pm 17dBm; \Delta V_{ac40} \approx \pm 10Mb/s;$$
$$\delta_{ac80} \approx \pm 20dBm; \Delta V_{ac80} \approx \pm 10Mb/s.$$

Therefore, presence of various architectural obstacles results in the same nature of influence, which depends on the thickness and density of the material, which is used for this purpose. This statement is correct on the condition that the level of the signal power does not fall below a certain threshold value. Therefore, in this case it is possible to state that architectural obstacles have a character of the additive coefficient of influence upon the efficiency parameters of the wireless channels of the family of 802.11x standards for the 5GHz frequency band.

On the basis of formula 1, as well as in accordance with the obtained results of experimental study, it is possible to determine the efficiency coefficient of the wireless channel for each situation under investigation with the help of the method of mathematical regression. In this case, it is possible to write the general mathematical model for estimation of the efficiency parameters as follows:

$$V(l) \approx -u \cdot l + s, \tag{3}$$

$$V_{pl}(l) \approx -hl + x, \tag{4}$$

where u, h are attenuation coefficients of characteristics (dimensionality of which is Mb/m); s and x are initial coefficients of the efficient rate of transmission and carrying capacity of a channel, respectively; l – length of the wireless channel or length of the radio circuit.

Taking into account the conception of construction of the multiservice networks, as well as the mechanism, which ensures quality of provision of the information-and-communication services [13], the parameter of the efficient rate of information transmission must be determined by the minimum value of fluctuations within the confidence interval. Then, it is possible to write the efficiency coefficient of the wireless channel in the following manner:

$$K \approx \frac{s - u \cdot l - \Delta V}{V_{pl.\max}}, \tag{5}$$

Coefficient of change of the carrying capacity of a channel is determined as follows:

$$K_{pl} \approx \frac{x - hl}{V_{pl.\max}}, \tag{6}$$

With the help of method of averaging the estimation of fluctuations of the obtained characteristics, it is possible to determine attenuation coefficients of the regression results. These results are presented in Table 1.

Table 1

Values of Attenuation Coefficients of the Efficiency Parameter Characteristics

	802.11a	802.11n 20MHz	802.11n 40MHz	802.11ac 20MHz	802.11ac 40MHz	802.11ac 80MHz
	Open space					
u	0.04	0.9	1.1	0.04	0.5	0.4
h	2.2	7	6	4.7	2.5	9
	Single door					
u	0.16	0.8	1.3	1.1	1.5	1.6
h	1.6	3.45	6.2	6	7	15
	Two doors					
u	0.24	0.7	1.5	0.6	0.3	0.4
h	1.84	5.7	10	4.5	8.2	12
	Walls					
u	0.7	1.3	2.6	1.8	2.1	2.76
h	2.1	5.5	6.8	5.2	7.6	9.2

From the obtained results it follows that attenuation coefficients of characteristics can have an average value for all standards. Difference between standards will be determined with the help of the interval of deviations and initial coefficients s and x. In order to obtain general estimation of the efficiency coefficient, the statement of the boundary of permissible variations is introduced for the attenuation coefficients. To this end, the following condition is written:

$$u = \frac{1}{n}\sum_{i=1}^{n} u_з \pm \Delta u, \tag{7}$$

$$h = \frac{1}{n}\sum_{i=1}^{n} h_з \pm \Delta h, \tag{8}$$

where Δu, Δh are the coefficients, which determine the boundaries of the permissible variations for the attenuation coefficients.

Having substituted the averaged values of regression and taking into account the permissible fluctuations, we will obtain:

$u = 1.3 \pm 1.4$ (*Mb/m*), $h = 8 \pm 6.5$ (*Mb/m*).

Therefore, taking into account the architectural obstacles within the premises, it is possible to write the efficiency criterion for the wireless channels of the family of 802.11x standards for the 5GHz frequency band in the following manner:

$$K \approx \frac{s - (1,3 \pm 1,4) \cdot l - \Delta V}{V_{pl.\max}}, \tag{9}$$

$$K_{pl} \approx \frac{x-(8\pm 6,5)l}{V_{pl.\max}}. \qquad (10)$$

In order to check correctness of the obtained expressions, we will draw two charts of dependences between the efficiency coefficients for the wireless channels of the standard 802.11n in the 20MHz frequency band and permissible boundaries of change of the attenuation coefficients. Results are shown in Fig. 5.

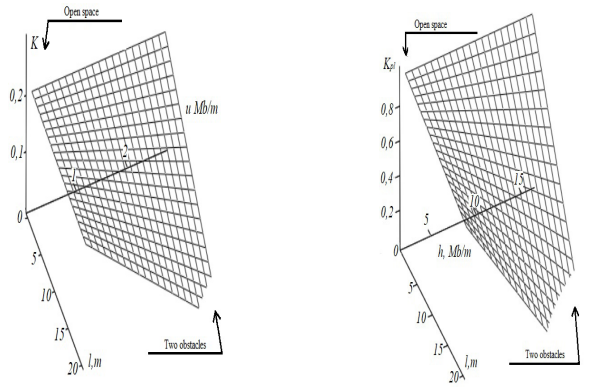

a **b**

Fig. 5. Dependences: a – of the efficiency coefficient of the wireless channel upon Δu; b – of the coefficient of change of carrying capacity upon Δh.

4. CONCLUSIONS

The following specific features have been determined on the basis of the obtained results of the study of the wireless channels of the family of 802.11x standards in the 5GHz frequency band:

- presence of physical obstacles increases the level of the signal fluctuations before the obstacle and following the obstacle (the higher density of obstacles, the higher attenuation of signals; therefore, the level of fluctuations increases);
- parameter of carrying capacity at the physical level is in direct dependence on the density of obstacles;
- channel of the standard 802.11a, whose characteristic of the efficient rate of information transmission is almost linear one, is the most stable channel, while channel 802.11ac in the 80MHz frequency band is the most unstable channel. This fact allows stating that utilisation of channels having higher frequency bands causes an increase in the efficient rate of information transmission;
- on the basis of the obtained study results, it is possible to assume that the architectural obstacle that has low density has low coefficient of signal attenuation.

REFERENCES

1. Rose, K., Eldridge, S., & Chapin, L. (2015). *The Internet of Things: An Overview.* The Internet Society (ISOC), 1–50. Available at https://www.internetsociety.org/wp-content/uploads/2017/08/ISOC-IoT-Overview-20151221-en.pdf
2. Perahia, E., & Stacey, R. (2013). *Next Generation Wireless LANs: 802.11n and 802.11ac.* Cambridge: Cambridge University Press.
3. Mykhalevskiy, D. (2014). Evaluation of wireless information transmission channel settings of 802.11 wi-fi standard. *Easten-European Journal of Enterprise Technologies*, *6/9*(72), 22–25. DOI: 10.15587/1729-4061.2014.31666.
4. Mykhalevskiy, D. (2017). Development of a spatial method for the estimation of signal strength at the input of the 802.11 standard receiver. *Eastern-European Journal of Enterprise Technologies*, *4/9*(88), 29–36. DOI: 10.15587/1729-4061.2017.106925.
5. Mykhalevskiy, D., Vasylkivskiy, N., & Horodetska, O. (2017). Development of a mathematical model for estimating signal strength at the input of the 802.11 standard receiver. *Eastern-European Journal of Enterprise Technologies*, *4/9*(88), 38–43. DOI: 10.15587/1729-4061.2017.114191.
6. Mykhalevskiy, D.V., & Huz, M.D. (2015). Estimation of the power distribution of the 802.11 standard transmitter in the room. *International periodic scientific journal Sword*, *1*(38), 48–52.
7. Deek, L., Garcia-Villegas, E., Belding, E., Lee, S. J., & Almeroth, K. (2011). The impact of channel bonding on 802.11n network management. *CoNEXT'11 Proceedings of the Seventh Conference on emerging Networking Experiments and Technologies 11,* 1–12.
8. Foster, K. (2007). Radiofrequency exposure from wireless LANs utilizing Wi-Fi technology. *Health Physics*, 280–289. Available at https://pdfs.semanticscholar.org/ffa4/af1900d204477c4640b390162456346faf10.pdf.
9. Mykhalevskiy, D.V., & Horodetska, O.S. (2015). Estimation of speed of transmission of information for the family of standards 802.11x in the range 2.4 GHz. *International periodic scientific journal Sword*, *3*(40), 43–47.
10. Chrysikos, T., & Kotsopoulos, S. (2013). Site-specific validation of path loss models and large-scale fading characterization for a complex urban propagation topology at 2.4 GHz. *Proceedings of the International MultiConference of Engineers and Computer Scientists, II*, 1–6.
11. Mykhalevskiy, D.V. (2016). Investigation of sensitivity impact of receiver to effective data transmission rate. *Proceedings of the 1st IEEE International Conference on Data Stream Mining & Processing*, Lviv, Ukraine, 369–372.
12. Aheeva, N.M., Lvovych, Y.Y., Shyian, P.L., & Mykhalevskiy, D.V. (2016). *Scientific Answers to Modern Questions: Technology in Technology* (2 volumes). Odessa: Kupryenko S.V.
13. Hertoghs, Y., & Maglione, R. (2014) Multi-service broadband network architecture. *Broadband Forum Marketing Report, MR-316*(1), 1–22.

802.11 STANDARTA BEZVADU KANĀLU IZPĒTE 5GHZ FREKVENČU JOSLĀ

D. V. Mihalevskijs

K o p s a v i l k u m s

Rakstā pētīti 802.11x ģimenes standartu bezvadu pārraides kanāli 5GHz frekvenču joslā, ņemot vērā arhitektūras šķēršļu ietekmi telpās. Par galvenajiem parametriem pētījuma gaitā ir izvēlēti šādi parametri: efektīvs datu pārraides ātrums, signāla jauda uztvērēja ieejā, kā arī kanāla caurlaides spēja. Eksperimentālā pētījuma rezultātā atbilstoša matemātiskā izteiksme atklāta, lai novērtētu 802.11x ģimenes standartu bezvadu kanālu efektivitātes kritēriju 5GHz frekvenču joslā, ņemot vērā attiecīgos arhitektūras šķēršļus telpās.

08.12.2018.

sciendo

LATVIAN JOURNAL OF PHYSICS
AND TECHNICAL SCIENCES
2019, N 1

DOI: 10.2478/lpts-2019-0005

INVESTIGATION OF THE INFLUENCE OF HIGH FREQUENCY ELECTROMAGNETIC FIELDS ON SORPTION PROCESSES

A. D. Galimbekov [1], M. A. Kadyrov [2], D. A. Drugov [3],
G. I. Muratova [4], M. A. Baizharikova [5]

[1] Department of Heat Power Engineering and Physics,
Bashkir State Agrarian University,
450001, 34 50th Anniversary of October Str., Ufa, Republic of Bashkortostan, RUSSIA
airbek@yandex.ru

[2, 3] Department of Geology of Oil and Gas Fields,
Tyumen Industrial University
625000, 56 Volodarskiy Str., Tyumen, RUSSIA
kadyrov-marsel@bk.ru
den.sub2016@yandex.ru

[4] Faculty of Information Technology, Automatic and Telecommunications,
Taraz State University named after M.Kh. Dulaty
010000, 60 Tole-bi Str., Taraz, KAZAKHSTAN
gaukhar70@mail.ru

[5] Department of Applied Informatics and Programming,
Taraz State University named after M.Kh. Dulaty
010000, 60 Tole-bi Str., Taraz, KAZAKHSTAN
marina.2288@mail.ru

The present paper studies the effect of high frequency electromagnetic fields on sorption processes. The equation of sorption kinetics describes the main mechanisms of the above effect. This can serve as the basis for more effective high frequency electromagnetic field technology to increase oil recovery by reducing adsorption of oil components on the porous bed skeleton.

Keywords*: adsorption, high frequency electromagnetic field, porous structure*

1. INTRODUCTION

It is known that adsorption layers of polar oil components are formed on the porous channel surfaces at oil filtration in a porous medium. These layers change the

molecular nature of solid surface and serve as a basis to form oil boundary layers whose viscosity exceeds that of oil in the bulk by an order of magnitude and whose thickness is commensurable with porous channel radius in a number of cases. Due to deposition of oil adsorption layers, the cross-section of filtration channels of porous medium is reduced, its penetrability decreases and, as a result, oil recovery of the porous bed drops [1], [2].

One of the promising technologies used to extract film oil adsorbed in the bed is based on application of high frequency electromagnetic fields (HF EMF). However, the mechanisms of HF EMF action on sorption processes still remain little studied. That is why theoretical studies in this area are very topical.

The objective of the present study is the theoretical investigation of the effect of HF EMF on sorption processes.

2. THE FEATURES OF FILTRATION OF A MONOPHASE SINGLE-COMPONENT SYSTEM IN POROUS MEDIUM

Let us consider filtration of a monophase single-component system in a porous medium at HF EMF action (with allowance made for sorption processes) within the framework of the "impurity" theory presented in [3]–[6]. It is assumed that the system contains a solute (impurity). Impurity absorption by the porous medium skeleton will be named sorption, bearing in mind impurity adsorption on the skeleton surface. The impurity mass concentration will be denoted by c_{imp}; the mass concentration of adsorbate (part of impurities sorbed on the pore surface) will be denoted by a.

We take the system as a solution whose density is a sum of the solvent and impurity densities:

$$\rho = \rho_s + \rho_{imp} = \rho(c_s + c_{imp}). \tag{1}$$

Here ρ_s, c_s, ρ_{imp} and c_{imp} are the densities and mass concentrations of solvent and impurity (dissolved in solution), respectively; ρ is the total medium density. HF EMF acting on the considered system is

$$\vec{E} = \vec{E}_0(\vec{r})\exp(i\omega t), \qquad \vec{H} = \vec{H}_0(\vec{r})\exp(i\omega t). \tag{2}$$

Here $\vec{E}_0(\vec{r})$ and $\vec{H}_0(\vec{r})$ are amplitudes of the electric and magnetic field strengths, respectively; ω is the HF EMF angular frequency; i is the imaginary unit; $\vec{r}$ is the radius vector of material continuum point.

Let us assume that the system under investigation is a nonmagnetic dielectric with low conductivity. The considered problem deals with the materials of oil technology, so the corresponding equations of state are as follows:

$$\vec{D} = \varepsilon_0 \varepsilon_{ef} \vec{E}, \qquad \vec{B} = \mu_0 \vec{H}, \tag{3}$$

$$\varepsilon_{ef} = (1-m)\varepsilon_{sk} + m\varepsilon \tag{4}$$

$$\varepsilon = \varepsilon'(\omega, c_s, c_{imp}, a, \rho, T) - i\varepsilon''(\omega, c_s, c_{imp}, a, \rho, T). \tag{5}$$

Here $\vec{D}$ and $\vec{B}$ are vectors of electric and magnetic induction, respectively; ε_0 and μ_0 are the electric and magnetic constants, respectively; ε_{ef} is the medium dielectric permittivity; m and ε_{sk} are skeleton porosity and dielectric permittivity, respectively; ε is dielectric permittivity of solvent with impurity; ε' and ε'' are the real and imaginary parts of the above dielectric permittivity.

3. ANALYSIS OF THE HENRY ADSORPTION

Let us obtain the sorption kinetics equation. In this case, the Henry adsorption will be considered, so we have to determine equilibrium conditions for the impurity in solution and part of impurity adsorbed on the pore surface. Based on thermodynamics of irreversible processes, the effect of HF EMF on chemical reactions in multicomponent media was studied and the *Guldberg*–Waage equation generalized to the case of HF EMF action was obtained in [7]–[9]. Considering adsorption as a variety of chemical reaction, (according to [7]–[9]) the *Guldberg*–Waage mass action equation may be presented as follows:

$$\frac{N_{ad}}{N_0} = K^*, \tag{6}$$

$$K^* = K_0 \exp\left(-\frac{E'_A - E''_A}{RT}\right), \tag{7}$$

$$\begin{aligned} E'_A &= E'_{Am} + \frac{\varepsilon_0 E_0^2 M}{4\rho}\left(\frac{\partial}{\partial a}\left(\varepsilon' - \omega\frac{\partial \varepsilon'}{\partial \omega}\right)\Big|_{\xi=\xi_0}\right), \\ E''_A &= E''_{Am} + \frac{\varepsilon_0 E_0^2 M}{4\rho}\left(\frac{\partial}{\partial c_{imp}}\left(\varepsilon' - \omega\frac{\partial \varepsilon'}{\partial \omega}\right)\Big|_{\xi=\xi_0}\right). \end{aligned} \tag{8}$$

Here $N_{ad} = \dfrac{n_{ad}}{n_0 + n_{ad}}$ is the mole fraction of adsorbate; $n_{a\partial} = \dfrac{m_{a\partial}}{M} = \dfrac{1}{M}\int\limits_V \rho a \, dV$ is the number of adsorbate moles in a selected medium volume; $n_0 = \dfrac{m_o}{M} = \dfrac{1}{M}\int\limits_V \rho m c_{imp\,0} \, dV$

is an equilibrium number of impurity moles in solution in the selected medium volume; $N_0 = \dfrac{n_0}{n_0 + n_{ad}}$ is an equilibrium mole fraction of impurity solved in solution; $c_{imp\,0}$ is an equilibrium mass concentration of impurity in solution; M is impurity mole mass; E'_A is activation energy of direct chemical reaction at HF EMF action (adsorption); E''_A is activation energy of back chemical reaction at HF EMF action desorption; K^* is the adsorption equilibrium constant.

Therefore, Eq. (6) can be rewritten as follows:

$$\frac{a}{m\,c_{imp\,0}} = K^* \tag{9}$$

from which

$$c_{imp\,0} = \frac{a}{K^* m} = \frac{a}{\gamma} = \frac{a}{\gamma_0}\exp\left(-\frac{Q}{R}\left(\frac{1}{T} - \frac{1}{T_0}\right)\right) \tag{10}$$

or

$$a = \gamma\, c_{imp\,0} = \gamma_0 \exp\left(\frac{Q}{R}\left(\frac{1}{T} - \frac{1}{T_0}\right)\right) c_{imp\,0}\,. \tag{11}$$

Equation (11) is the Henry law generalized to the case of HF EMF action; γ is the Henry coefficient equal to

$$\gamma = K^* m = K_0 m \exp\left(-\frac{E'_A - E''_A}{RT}\right) = K_0 m \exp\left(-\frac{Q}{RT}\right) = \gamma_0 \exp\left(\frac{Q}{R}\left(\frac{1}{T} - \frac{1}{T_0}\right)\right). \tag{12}$$

Here $\gamma_0 = K_0 m \exp\left(\dfrac{Q}{RT_0}\right)$ is the Henry constant value at $T = T_0$; $Q = Q_m + Q^{em}$ is the adsorption heat; $Q_m = E''_{Am} - E'_{Am} > 0$ is adsorption heat without regard for HF EMF action; $Q^{em} = \dfrac{\varepsilon_0 E_0^2 M}{4\rho}\left(\dfrac{\partial}{\partial c_{imp}}\left(\varepsilon' - \omega\dfrac{\partial\varepsilon'}{\partial\omega}\right)\Big|_{\xi=\xi_0} - \dfrac{\partial}{\partial a}\left(\varepsilon' - \omega\dfrac{\partial\varepsilon'}{\partial\omega}\right)\Big|_{\xi=\xi_0}\right)$ is adsorption heat due to HF EMF action.

On the other hand, the rate of adsorbate mass variation in the selected volume of a porous medium is proportional to the difference $(m\rho c_{imp} - m\rho c_{imp\,0})$:

$$\frac{\partial}{\partial t}\int_V \rho a\, dV = \beta \int_V \left(m\rho c_{imp} - m\rho c_{imp\,0}\right) dV\,, \tag{13}$$

where $\beta = \beta_m + \beta^{em}$ is the adsorption rate; β_m is the adsorption rate independent of HF EMF; β^{em} is the adsorption rate dependent on HF EMF.

Thus, after some transformations, we get the sorption kinetics equation:

$$\frac{\partial \rho a}{\partial t} = m\rho(\beta_m + \beta^{em}) \cdot \left(c_{imp} - a\gamma_0^{-1} \exp\left(-\frac{Q_m + Q^{em}}{R} \cdot \left(\frac{1}{T} - \frac{1}{T_0} \right) \right) \right). \tag{14}$$

4. ANALYSIS OF MECHANISMS OF HF EMF INFLUENCE ON SORPTION KINETICS

By analysing the sorption kinetics equation (Eq. (14)), the following mechanisms of HF EMF influence on sorption kinetics can be distinguished:

1. The heat mechanism of HF EMF action: at this action, the medium is heated due to dielectric losses. As the Henry coefficient (Eq. (12)) depends on temperature, this results in displacement of the adsorption equilibrium curve [10]–[13]. The Henry coefficient decreases as temperature grows; so the desorption processes prevail. One can exert control over intensity of medium heating by choosing HF EMF frequency.
2. The HF EMF influence on sorption kinetics via adsorption heat: an additional electromagnetic component Q^{em} appears in the expression for adsorption heat at HF EMF action [14]. There are two special cases that can be implemented depending on the HF EMF frequency:
   - 2.1. $Q^{em} > 0$; in this case, adsorption heat increases. This leads to growth of the Henry coefficient and thus to predominance of adsorption processes.
   - 2.2. $Q^{em} < 0$; in this case, adsorption heat decreases. This leads to reduction of the Henry coefficient and thus to predominance of desorption processes.
3. The HF EMF influence on the rate of sorption processes: an electromagnetic part β^{em} appears in the expression for adsorption rate at HF EMF action. There are also two special cases that can be implemented depending on the HF EMF frequency:
   - 3.1. $\beta^{em} > 0$; in this case, the adsorption rate increases and the system goes to adsorption equilibrium more quickly.
   - 3.2. $\beta^{em} < 0$; in this case, the adsorption rate decreases and the system goes to adsorption equilibrium more slowly.

5. CONCLUSION

A theoretical study of the effect of HF EMF on sorption processes has been carried out. It has been established that one can exert control over adsorption-

desorption processes by selectively choosing HF EMF power and frequency. The mechanisms of HF EMF action on sorption processes (the heat mechanism of HF EMF action, the HF EMF influence on sorption kinetics via adsorption heat, the HF EMF influence on the rate of sorption processes) considered in the present paper can form the basis of more efficient HF EMF technologies to increase oil recovery of porous beds by decreasing adsorption of oil components on the rock skeleton.

REFERENCES

1. Formalev, V.F., Kolesnik, S.A., & Kuznetsova, E.L. (2018). On the wave heat transfer at times comparable with the relaxation time upon intensive convective-conductive heating. *High Temperature, 56*(3), 393–397.
2. Kolesnik, S.A., Formalev, V.F., & Kuznetsova, E.L. (2015). On inverse boundary thermal conductivity problem of recovery of heat fluxes to the boundaries of anisotropic bodies. *High Temperature, 53*(1), 68–72.
3. Barenblatt, G.I., Entov, V.M., & Ryzhik, V.M. (1984). *Movement of liquids and gases in natural formations*. Moscow: Nedra.
4. Nikolaevsky, V.N. (1984). *Mechanics of porous and fissured media*. Moscow: Nedra.
5. Bondarev, E.A., & Nikolaevsky, V.N. (1962). Convective diffusion in porous media taking into account the adsorption phenomenon. *Applied Mechanics and Technical Physics*, *5*, 128–134.
6. Tlebayev, M.B., Tazhiyeva, R.N., Doumcharieva, Zh.E., Aitbayeva, Z.K., & Baijarikova, M.A. (2017). Mathematical research of the accelerated three-stage process of substrate fermentation in bioreactors. *Journal of Pharmaceutical Sciences and Research*, *9*(4), 392–400.
7. Galimbekov, A.D. (2004). Influence of high-frequency electromagnetic field on chemical reactions in multicomponent media. *Journal of Physical Chemistry, 78*(9), 1693–1697.
8. Galimbekov, A.D. (2007). *Some aspects of the interaction of electromagnetic fields with polarizing media.* Thesis for the degree of Doctor of Physics and Mathematics. Ufa: Bashkir State University.
9. Kovaleva, L.A., & Galimbekov, A.D. (2004). Influence of a high-frequency electromagnetic field on physicochemical processes in multicomponent media. *Bulletin of the Orenburg State University, 1*(26), 141–146.
10. Coello-Fiallos, D.C., Espin-Lagos, S.M., Vacacela Gomez, C., Tavolaro, A., & Caputi, L.S. (2018). Comparison of pure membranes of 13X and 5A zeolite for removal of acridine orange dye from aqueous solutions. *Periódico Tchê Química, 15*(29), 251–257.
11. Cavallari, R.V., De Lima, N.B., Silva, J.C.M., Bergamashi, V.S., & Ferreira, J.C. (2018). Preparation of catalyst support from bio carbon. *Periódico Tchê Química, 15*(30), 115–122.
12. Vian, A., Davies, E., Gendraud, M., & Bonnet, P. (2016). Plant responses to high frequency electromagnetic fields. *Biomed Res Int., 2016,* 1830262.
13. D'Agostino, S., Monica, C.D., Palizzi, E., Di Pietrantonio, F., Benetti, M., Cannatà, D., … Ramundo-Orlando, A. (2018). Extremely high frequency electromagnetic fields facilitate electrical signal propagation by increasing transmembrane potassium efflux in an artificial axon model. *Scientific Reports, 8*, 9299.
14. Kıvrak, E.G., Yurt, K.K., Kaplan, A.A., Alkan, I., & Altun, G. (2017). Effects of electromagnetic fields exposure on the antioxidant defense system. *Journal of Microscopy and Ultrastructure, 5*(4), 167–176.

AUGSTFREKVENCES ELEKTROMAGNĒTISKO LAUKU IETEKMES IZPĒTE UZ SORBCIJAS PROCESIEM

A. D. Galimbekovs, M. A. Kadirovs, D. A. Drugovs,
G. I. Muratova, M. A. Baižarikova

K o p s a v i l k u m s

Šajā rakstā apskatīta augstfrekvences elektromagnētisko lauku ietekme uz sorbcijas procesiem. Sorbcijas kinētikas vienādojums apraksta galvenos minētā efekta mehānismus. Tas var kalpot par pamatu efektīvākai augstfrekvences elektromagnētiskā lauka tehnoloģijai, lai palielinātu eļļas atgūšanu, samazinot eļļas komponentu adsorbciju porainā gultnes skeletā.

12.11.2018.

sciendo

LATVIAN JOURNAL OF PHYSICS
AND TECHNICAL SCIENCES
2019, N 1

DOI: 10.2478/lpts-2019-0006

QUANTUM PHYSICS

ELECTRONIC PROCESSES IN SOLID STATE: DIRAC FRAMEWORK

E. Klotins
Institute of Solid State Physics, University of Latvia,
8 Kengaraga Str., Riga, LV-1063, LATVIA
klotins@cfi.lu.lv

The present paper proposes canonical Dirac framework adapted for application to the electronic processes in solid state. The concern is a spatially periodic structure of atoms distinguished by birth and annihilation of particle states excited due to interaction with the electromagnetic field. This implies replacing the conventional energy-momentum relation specific of the canonical Dirac framework and permissible for particle physics by a case specific relation available for the solid state. The advancement is a unified and consistent mathematical framework incorporating the Hilbert space, the quantum field, and the special relativity. Essential details of the birth and annihilation of the particle states are given by an illustrative two-band model obeying basic laws of quantum mechanics, special relativity, and symmetry principles maintained from the canonical Dirac framework as a desirable property and as a prerogative for the study of the particle coupling and correlation.

Keywords: *canonical quantization, Dirac field, Hilbert spaces, quasi-particle birth/annihilation*

1. INTRODUCTION

The long-standing challenge to describe charged particles in solids exposed by electromagnetic fields is how to incorporate the Hilbert space, the quantum field theory, and the special relativity into a consistent unified framework. Current theory for these processes is founded on the study of particle creation. In the original context, the key issue is an electromagnetic field sufficient to create pairs of photoexcited particles from vacuum in high-intensity laser experiments [1], [2]. Though the particle production from vacuum has yet to be experimentally verified, the electronic processes in solids brought benefits from a consistent description of quantum many-body phenomena far from equilibrium. Conventionally, for photoexcited particles created from vacuum in high-intensity laser experiments, we have a solution of the Dirac equation with the classical electromagnetic four-vector potential incorporated. Expanding these two fields in Fourier modes reveals that their wavelengths are much larger than the wavelength of the quantized modes of the Dirac field functions. The

physical picture is that in this case a photon of the classical four-vector potential does not resolve the quantum nature of the photoexcited electron. It allows the equations of motion for the observables and the slowly varying four-vector fields to be solved self-consistently at the long wavelength scale [3]. However, well-accepted solutions for a free particle and even for quantum fields comprise a quantity identified to the Einstein energy-momentum relation as an element of particle physics and violated in the solids. In this manuscript, we reconsider the energy-momentum relation making it case specific and available for solid-state applications. The viewpoint acquired from the Dirac framework is that physically acceptable solutions imply two mutually consistent equations: the first is Klein-Gordon type related to the Schrödinger equation, and the second is the modified Dirac equation.

Going beyond the canonical Dirac framework, we focus attention on a compound system constituted of the Schrödinger type Hamiltonians. The novelty we claim and the modification we propose is that the equation of motion for this compound system is consistent with the tensor product of its components. Emerging entities are both the expected energy-momentum relation and the (equation of motion for) joint wave function of the compound system.

Ongoing investigations were successful in the oscillator representation for the joint wave function of the compound system [4], [5], and in the mathematical technique for the creation and annihilation operators accepted in this work [6]. In the physics of semiconductors, the excitation of electron-hole pair has attracted much attention and was extensively studied in [7] and [8]. Central in these pioneering approaches is the composite system specified by macroscopic dispersion relations for noninteracting electrons and holes that appear as correlated in the momentum and energy. Charge conjugation of these particles with optical radiation is obtained within the framework of minimal substitution, which the electromagnetic vector potential considered as a macroscopic entity [9].

What we learn from the aforementioned references is that, certainly, the oscillator equation for the composite system is central and plays the role of the Klein-Gordon equation in the canonical Dirac theory, and the canonical Dirac equation, indeed, seems to be consistent with both relativity and even the probability interpretation for a single relativistic particle. What exactly is the challenge, is transition to more general energy-momentum relations spanned by the lattice environment with a variable number of particles. In this context, we give preference to the quantum field functions that a priori imply the Lorentz covariance and the quadratic dispersion of constituting particles. Under these conditions, the Lagrangian density for quantum field functions appears at once, encodes the parameters of macroscopic Hamiltonians, and is available for canonical quantization as desirable properties. This means that component of a composite system is not described independently by its own wave function, without consideration of the state of the other and, generally, arising as a result of interactions between the component degrees of freedom. Finally, as the main result of this work, we obtain a set of differential equations of birth and annihilation operators for an illustrative electron-hole model.

The manuscript is organised as follows. Section 2 presents a general introduction to the problem and some standard information on theory that is used later in the paper. In Section 3, we give details of the modified Dirac equation and the

associated quantum field functions. In Section 4, the Lagrangian density is built from the modified Dirac equation and available for the minimum action mathematical technique. Finally, Section 5 summarises the results of this study. We use natural units, $\hbar = c = 1$ restoring them explicitly where adding insight.

2. BASIC CONCEPTS AND DEFINITIONS

While the basis of quantum mechanics is provided through purely algebraic relations, for specific results a complementary representation of the Hilbert space, the quantum field theory and the special relativity are used. To bring rationale of all, a special attention is paid to the quantum mechanical wave functions defined so that the Hilbert space is given by a set of elements $H = \left(|\psi\rangle, |\varphi\rangle, |\chi\rangle, ...\right)$ obeying postulates for scalar product, linearity, completeness, and separability. This is definitely the case of Schrödinger type wave functions for Hamiltonians comprising both the kinetic and time independent potential energy terms. For arbitrary dimensionality, the joint wave function implies linearly independent vector spaces $V = \{v_1, v_2, v_3\}$ and $W = \{w_1, w_2, w_3\}$, where $\{\vec{e}_1, \vec{e}_2, ..., \vec{e}_n\}$ is the basis vectors of V, and similarly $\{\vec{f}_1, \vec{f}_2, ..., \vec{f}_m\}$ for W. The tensor product of the vector spaces $V \otimes W$ is spanned by the basis vectors $\vec{e}_i \otimes \vec{f}_j$ as given by relation

$$\vec{v} \otimes \vec{w} = \left(\sum_i^n v_i \vec{e}_i \right) \otimes \left(\sum_j^m w_j \vec{f}_j \right) = \sum_i^n \sum_j^m v_i w_j \left(\vec{e}_i \otimes \vec{f}_j \right) . \tag{1}$$

We categorize this property as a fundamentally new multi-particle approach available for the creation and annihilation of particle states in far-from-equilibrium conditions.

Consequences for the Dirac framework [10] are that instead of the prototypical Klein-Gordon equation for a free relativistic particle we have the oscillator equation for the case specific energy-momentum relation. The associated Dirac equations for spinor functions turn into a modified Dirac equation distinguished by first order in space and time derivatives and by numerical coefficients connecting it with the oscillator equation. Requested consistence between both equations is fully defined by drawing comparison between their differential operators of appropriate order. Necessary restrictions of the special relativity are encoded in appropriate quantum field functions. This allows the Lagrange and Hamilton transition from the joint wave function of the composite system to the Lagrangian density for the canonically quantized field operators of the Hamiltonian density and the methods of quantum statistics available.

The observable quantities emerge in a standard way as integrals over time-dependent distribution functions, however, being beyond the scope of this manuscript.

3. BUILDING THE MODIFIED DIRAC EQUATION

In this section, we follow the canonical Dirac framework distinguished by the wave equation that is first order in both space and time derivatives and linear in the momentum

$$\left(\hat{E} - \overline{\alpha} \cdot \vec{p} - \beta m\right)\Psi(x) = 0\,, \tag{2}$$

where, conventionally, solutions for the entities $\overline{\alpha}$ and β imply drawing a comparison between the Dirac equation (2) and the Klein-Gordon equation [11].

The concern is the momentum-energy relation of composite systems given implicitly by the tensor product mathematical technique. As an example, we present a two-band model specified by the conduction and valence states as well as by width of the band gap. We set the Dirac equation (2) modified for the electron and the hole as

$$\left(i\hbar\frac{\partial}{\partial t} + i\hbar\overline{\alpha}\cdot\vec{\nabla} + i\hbar\overline{\gamma}\cdot\vec{\nabla} - \beta\frac{\Delta}{2}\right)\Psi(x) = 0\ . \tag{3}$$

Here the constraints on the constants $\overline{\alpha}$, $\overline{\gamma}$ and β follow from drawing a comparison between the (i) extended Dirac equation (3) squared and (ii) the oscillator equation.

We build the constituting equations for the prototypic composite system making use of the macroscopic constituting Hamiltonians H_c and H_v as

$$H_{c/v} = \pm\mathbf{p}^2/\left(2m_e\right) \pm \Delta/2\ , \tag{4}$$

where the momentum $\mathbf{p}$ and the (electronic) band gap Δ are classical quantities. Quantization of classical dynamic quantities implies the energy operator $\hat{E} \to i\,\mathrm{h}\partial_t$ and the momentum operator $\hat{\mathbf{p}} \to -i\,\mathrm{h}\nabla$. Finally, the equation of motion for this composite system (oscillator equation) is built up by tensor product (1) at $m = n = 3$ as

$$\left(\overset{\mathrm{r}}{v} \otimes \overset{\mathrm{r}}{w}\right)\Psi\left(\mathbf{x},t\right) = 0\cdot \tag{5}$$

Treatment of the tensor product implies components of the vector spaces V and W in the operator representation as $v = \hat{E}_c - \Delta/2 - \varepsilon_c(\hat{\mathbf{p}})$ and $w = \hat{E}_v + \Delta/2 + \varepsilon_v(-\hat{\mathbf{p}})$ gives the expected oscillator equation for the composite system as

$$\left(-\frac{\Delta^2}{4} + \hat{E}^2 - \frac{\Delta}{2}\varepsilon_c\left(\hat{\mathbf{p}}\right) - \hat{E}\varepsilon_c\left(\hat{\mathbf{p}}\right) - \frac{\Delta}{2}\varepsilon_v\left(-\hat{\mathbf{p}}\right) + \hat{E}\varepsilon_v\left(-\hat{\mathbf{p}}\right) - \varepsilon_c\left(\hat{\mathbf{p}}\right)\varepsilon_v\left(-\hat{\mathbf{p}}\right)\right)\Psi\left(\mathbf{x},t\right) = 0\,. \tag{6}$$

3.1 SQUARED REPRESENTATION OF THE MODIFIED DIRAC EQUATION

In this subsection, we are drawing comparison between the Dirac equation (4) squared and the oscillator equation (6) resulting in the relations for the coefficients α, γ and β as $\alpha_x^2 = \alpha_y^2 = \alpha_y^2 = -\Delta/(4m_e)$, $\gamma_x^2 = \gamma_y^2 = \gamma_z^2 = -\Delta/(4m_h)$ and $\beta^2 = \mathbf{1}$. The mixed projections of $\overline{\alpha}$ and $\overline{\gamma}$ satisfy anticommutation relations $\alpha_j\alpha_k + \alpha_k\alpha_j = 0$ and $\gamma_j\gamma_k + \gamma_k\gamma_j = 0$ at $j,k = x,y,z$, $j \neq k$. The anticommutation relations of $\overline{\alpha}\beta$ type is $\left(\beta\alpha_j + \alpha_j\beta\right) = 0;\quad j = x,y,z$ and of $\overline{\gamma}\beta$ type is $\left(\beta\gamma_j + \gamma_j\beta\right) = 0;\ j = x,y,z$. These anticommutation relations imply that at least for the illustrative two-band model the classical Dirac $\overline{\alpha}$ – matrices given by relation $\alpha_x^2 = \alpha_y^2 = \alpha_z^2 = \mathbf{1}$ and supporting anticommutation conditions in the canonical Dirac framework are violated. Instead, the anticommutation conditions must be encoded in the appropriate quantum field function(s).

The same concern is for the $\overline{\gamma}$ – factor in (3). The consequences for the mixed projections of $\overline{\alpha\gamma}$ are that all of it turns to zero and the similarity with canonical anticommutation relations [11] is definitely formal. As a result, the full solution of (11) implies explicit relations $\overline{\alpha} = \sqrt{-\Delta/(4m_e)}$, $\overline{\gamma} = \sqrt{-\Delta/(4m_e)}$.

The unknown yet overall wave function must obey the Fourier mode expansion as

$$\Psi(x) = \int dp^4 \left(2\pi\right)^{-4} \tilde{\Psi}\left(p\right) exp\left(-ipx\right), \tag{7}$$

where properties of the composite system are encoded in the momentum space field $\widetilde{\Psi}(p)$ and the 4-vector scalar product $px = Et/\hbar - \mathbf{p}\cdot\mathbf{x}/\hbar$ is in the $\{+,-,-,-\}$ metric signature. In full detail, the Dirac equation (3) is written in differential operators as

$$\begin{aligned} &-\frac{\Delta}{2}\Psi + i\hbar\Psi_t + \left(i\hbar\alpha_z\Psi_z + i\hbar\alpha_y\Psi_y + i\hbar\alpha_x\Psi_x\right) \\ &+\left(i\hbar\gamma_z\Psi_z + i\hbar\gamma_y\Psi_y + i\hbar\gamma_x\Psi_x\right) = 0 \end{aligned} \tag{8}$$

where the spatial gradient terms are included in brackets. Finally, implementing (7) in (8) turns the equation of motion for the overall quantum wave function of composite system as

$$\frac{\Delta}{2}\Psi - \left(\sqrt{2\Delta\varepsilon_e\left(\mathbf{p}\right)} + \sqrt{2\Delta\varepsilon_h\left(-\mathbf{p}\right)}\right)\Psi + i\hbar\dot{\Psi} = 0\,. \tag{9}$$

3.2 QUANTUM FIELD FUNCTIONS

Extensions of (9) to more realistic systems interacting with external fields and exhibiting variable number of excited states require transition from quantum field functions to the quantum operator functions. The search is, first, the Lorentz invariance

[12] and the four Fourier representations of field functions related to positive (conduction) and negative (valence) energy states and, second, harmonization of the relativistic invariant integration measure with the macroscopic dispersion relations of the electrons and holes. To this end, we apply the Lorentz invariant representation for quantum field functions as [12].

$$\Psi(x) = \int d^4 p (2\pi)^{-4} \tilde{\Psi}(p) \exp(-ipx), \tag{10}$$

$$\Psi^*(x) = \int d^4 p (2\pi)^{-4} \tilde{\Psi}^*(p) \exp(ipx), \tag{11}$$

where after (1), (2) the momentum space field is given by expansion in δ – functions as

$$\begin{aligned} &\tilde{\Psi}(E,\mathbf{p}) \to \\ &\delta\left[E - \frac{\Delta}{2} - \varepsilon_c(\mathbf{p})\right]\left[E + \frac{\Delta}{2} + \varepsilon_v(-\mathbf{p})\right]\psi(E,\mathbf{p}) = \delta g(E,\mathbf{p})\psi(E,\mathbf{p}) \end{aligned}, \tag{12}$$

$$\begin{aligned} &\tilde{\Psi}^*(E,\mathbf{p}) \to \\ &\delta\left[E - \frac{\Delta}{2} - \varepsilon_c(\mathbf{p})\right]\left[E + \frac{\Delta}{2} + \varepsilon_v(-\mathbf{p})\right]\psi^*(E,\mathbf{p}) = \delta g(E,\mathbf{p})\psi^*(E,\mathbf{p}) \end{aligned}. \tag{13}$$

Equations (12), (13) support the necessary connection between the macroscopic parameters of the compound system and the quantum field functions (10), (11).

Optical radiation implies a spatially homogeneous time-dependent electric field, represented (at appropriate wavelength) by the vector potential in the Coulomb gauge $\nabla \cdot \mathbf{A} = 0$. In full, the momentum space field contributes as a replacement $\mathbf{p} \to \mathbf{p} \pm \mathbf{A}(t)$ in quantum field functions, in the Lagrangian density, and, finally, in the birth and annihilation operators of associated quasiparticles, here – electrons and holes. However, this desirable property involves complexities, and, in this illustrative example, we restrict the calculations in free field mode, restating the effect of time-dependent electric field in the final relations.

Going over the technicalities for connection between the macroscopic parameters of the compound system and the quantum field functions (10), (11) we write the expected field functions decomposed in sums over momentum $\mathbf{p}$

$$\Psi(\mathbf{x},t) = \frac{1}{L^{3/2}} \sum_{\mathbf{p}} \left(\frac{1}{\sqrt{\Delta + \varepsilon_c(\mathbf{p}) + \varepsilon_v(-\mathbf{p})}} \left(a_{e,\mathbf{p}} e^{-i\left(\frac{\Delta}{2} + \varepsilon_c(\mathbf{p})\right)t} + a_{h,-\mathbf{p}} e^{i\left(\frac{\Delta}{2} + \varepsilon_v(-\mathbf{p})\right)t} \right) \right) e^{i\mathbf{p}\mathbf{x}}, \tag{14}$$

$$\Psi^*(\mathbf{x},t) = \frac{1}{L^{3/2}} \sum_{\mathbf{p}} \left(\frac{1}{\sqrt{\Delta + \varepsilon_c(\mathbf{p}) + \varepsilon_v(-\mathbf{p})}} \left(a^*_{c,\mathbf{p}} e^{+i\left(\frac{\Delta}{2} + \varepsilon_c(\mathbf{p})\right)t} + a^*_{v,-\mathbf{p}} e^{-i\left(\frac{\Delta}{2} + \varepsilon_v(-\mathbf{p})\right)t} \right) \right) e^{-i\mathbf{p}\mathbf{x}}. \tag{15}$$

4. LAGRANGE AND HAMILTON FORMALISM

The Lagrange and Hamilton formalism implies mathematical abstractions regarded to the fundamentals of quantum electrodynamics, whereas on physical grounds the expectations is to describe evolution of the particle distribution functions during the external field evolution. Having the Lorentz invariant quantum field functions (10), (11) we accept that sufficient condition for the Lagrangian density to have physical sense is to return the modified Dirac equation (8), (9). To this end we set the Lagrangian density for the quantum field functions (14), (15) as

$$L = \frac{\Delta}{2}\Psi\Psi^* - \left(\sqrt{2\Delta\varepsilon_e(\vec{p})} + \sqrt{2\Delta\varepsilon_h(-\vec{p})}\right)\Psi\Psi^* + i\hbar\Psi^*\dot{\Psi} - i\hbar\dot{\Psi}^*\Psi + \frac{\hbar^2}{\Delta}\dot{\Psi}^*\dot{\Psi}. \tag{16}$$

The canonically conjugate momentum fields read in usual way as

$$\pi(\vec{x},t) := \frac{\partial L}{\partial\dot{\Psi}(\vec{x},t)} \to \sum_{\mathbf{p}}\left(i\hbar\Psi^* + \frac{\hbar^2}{\Delta}\dot{\Psi}\right), \tag{17}$$

$$\pi^*(\vec{x},t) := \frac{\partial L}{\partial\dot{\Psi}^*(\vec{x},t)} \to \sum_{\mathbf{p}}\left(-i\hbar\Psi + \frac{\hbar^2}{\Delta}\dot{\Psi}\right), \tag{18}$$

and the free field Hamiltonian density is given by

$$\begin{aligned} &H_{tot} = \sum_{\mathbf{p}}\left(\pi(\vec{x},t)\dot{\Psi} + \pi^*(\vec{x},t)\dot{\Psi}^* - L\right) \to \\ &\sum_{\mathbf{p}}\left(\left(-\frac{\Delta}{2} + \sqrt{2\Delta\varepsilon_e(\vec{p})} + \sqrt{2\Delta\varepsilon_h(-\vec{p})}\right)\Psi\Psi^* + \frac{\hbar^2}{\Delta}\dot{\Psi}\dot{\Psi}^*\right) \end{aligned} \tag{19}$$

Implementation of the quantum field functions (14), (15) in (19) gives the free field Hamiltonian density in quasiparticle representation as

$$H_{tot} = \frac{1}{V}\sum_{\mathbf{p}}\left(\begin{array}{l} \dfrac{\Delta\varepsilon_c(\mathbf{p}) + \varepsilon_c(\mathbf{p})^2 - \left(\frac{\Delta}{2}\right)^2 + \sqrt{2\Delta\varepsilon_e(\mathbf{p})} + \sqrt{2\varepsilon_v(-\mathbf{p})}}{\Delta + \varepsilon_c(\mathbf{p}) + \varepsilon_v(-\mathbf{p})} a_e(\mathbf{p})a_e^*(\mathbf{p}) + \\ \dfrac{\Delta\varepsilon_v(-\mathbf{p}) + \varepsilon_v(-\mathbf{p})^2 - \left(\frac{\Delta}{2}\right)^2 + \sqrt{2\Delta\varepsilon_e(\mathbf{p})} + \sqrt{2\varepsilon_v(-\mathbf{p})}}{\Delta + \varepsilon_c(\mathbf{p}) + \varepsilon_v(-\mathbf{p})} a_h(-\mathbf{p})a_h^*(-\mathbf{p}) \end{array}\right) \tag{20}$$

that is available for the minimal action treatment. The factors before the creation and annihilation operators in (20) are functions of the macroscopic parameters of the compound system as desirable property.

The necessary equations of motion for the creation and annihilation operators, implies the quantum field functions (14), (15) in the canonical quantized fashion as

$$\Psi(\mathbf{x},t)=\frac{1}{\sqrt{V}}\sum_{\mathbf{p}}\left(\frac{\sqrt{\Delta}}{\sqrt{\Omega(\mathbf{p},t)}}\left(a_e(\mathbf{p},t)+a_h(-\mathbf{p},t)\right)\right)e^{i\mathbf{px}}\,, \tag{21}$$

$$\Psi^{\dagger}(\mathbf{x},t)=\frac{1}{\sqrt{V}}\sum_{\mathbf{p}}\left(\frac{\sqrt{\Delta}}{\sqrt{\Omega(\mathbf{p},t)}}\left(a_c^{\dagger}(\mathbf{p},t)+a_v^{\dagger}(-\mathbf{p},t)\right)\right)e^{-i\mathbf{px}}\,. \tag{22}$$

Then, going back to the canonically conjugate momentum fields (17), (18) we turn to the standard definition

$$L=\pi\dot{\Psi}+\pi^{*}\dot{\Psi}^{*}-H_{tot}\,. \tag{23}$$

where the Lagrangian density (23) is consistent with the integrand of the minimal action relation $S=\int dx\,L$ and the equations of motion are given by functional derivatives over the time dependent amplitudes $a_{e,h}(\mathbf{p},t)$.

Parameters of the compound system are encoded by factor $\Omega(\mathbf{p},t)=\Delta+\varepsilon_c(\mathbf{p},t)+\varepsilon_v(-\mathbf{p},t)$ and the dispersions are given by (3), (4). Similarly to [7], extensions of the free field relations to the case of electromagnetic radiation is obtained by the replacement $\mathbf{p}\to\mathbf{p}\pm\mathbf{A}(t)$ in quantum field functions (21, (22).

5. CONCLUSIONS

In this manuscript, the canonical Dirac framework is adapted for application to the electronic processes in solid state. The advancement is in replacing the conventional energy-momentum relation permissible for particle physics by a case specific relation available for solid-state applications. As a result, a complementary representation of the Hilbert space, the quantum field theory and the special relativity are applied. Emerging entities are both the expected case specific energy-momentum relation and the (equation of motion for) joint wave function of the compound system of particles. We claim that this result is original, previously unpublished, and from the best of our knowledge no such modification of Dirac theory is published elsewhere. Because of application to solid state and as an illustration of the proposed modification of the canonical Dirac framework, the electron-hole pair is discussed in full detail.

While conventionally we are concerned with fermionic particles, the modified Dirac framework describes fields on a level where the particles are not there from

the start. It is only if to solve the field equations in presence of a pulse of external field that gives rise to the emergence of quasiparticles. This desirable property is a prerogative for strong coupling and correlation approaches having come to the fore of modern condensed matter physics.

ACKNOWLEDGEMENTS

The present research has been supported by the Institute of Solid State Physics, the University of Latvia in the frames of the ERA-NET HarvEnPiez project (No. ES RTD/2016/15).

REFERENCES

1. Di Piazza, A., Müller, C. K., Hatsagortsyan, Z., & Keitel, C. H. (2012). Extremely high-intensity laser interactions with fundamental quantum systems. *Rev. Mod. Phys., 84*, 1177.
2. Poder, K., Tamburini, M., Sarri, G., Di Piazza, A., Kuschel, S., Baird, C. D., & Zepf, M. (2018). Experimental signatures of the quantum nature of radiation reaction in the field of an ultraintense laser, *Phys. Rev. X 8*, 031004.
3. Hegelich, B. M., Labun, L., & Labun, O. Z. (2017) Finding quantum effects in strong classical potentials. *J.Plasma Phys., 83*(3), 595830301.
4. Pervushin, V.N., & Skokov, V.V. (2006). Kinetic description of fermion production in the oscillator representation, *Acta Physica Polonica B*, *37*(9), 2587–2600.
5. Pervushin, V. N., Skokov, V. V., Reichel, A. V., Smolyansky, S. A., & Prozorkevich, A. V. (2005). The kinetic description of vacuum particle creation in the oscillator representation. *International Journal of Modern Physics A, 20*(24), 5689–5704.
6. Friesen, A.V., Prozorkevich, A.V. , Smolyansky, S.A., & Bonitz, M. (2007). Nonperturbative kinetics of electron-hole excitations in strong electric field. In *Saratov Fall Meeting 2006: Laser Physics and Photonics, Spectroscopy and Molecular Modeling VII,* eds. V.L. Derbov, L.A. Melnikov, and L.M. Babkov, Proc. SPIE 6537, article id. 653707.
7. Smolyansky, S.A., Bonitz, M., & Tarakanov, A.V. (2010). Strong field generalization of the interband transitions kinetics. *Physics of Particles and Nuclei*, *41*(7), 1075–1078.
8. Smolyansky, S. A., Panferov, A. D., Blaschke, D. B., Juchnowski, L., K ̈ampfer, B., & Otto, A. (2017). Vacuum particle-antiparticle creation in strong fields as a field induced phase transition. *Russ. Phys. J., 59*(11), 1731–1738.
9. Panferov, A. D., Smolyansky, S. A., Titov, A. I., Kaempfer, B., Otto, A., Blaschke, D. B., & Juchnowski, L. (2017). Field induced phase transition in the few photon regime, *EPJ Web Conf*., *138*, 07004.
10. Dirac, P. (1928). The quantum theory of the electron. *Proc. R. Soc. Lond*., A117, 610–634.
11. Thomson, M. (2013). *Modern particle physics*. Cambridge: Cambridge University Press.
12. Álvarez-Gaumé, L., & Vázques-Mozo, M. Á. (2012). An invitation to quantum field theory. Lecture Notes in Physics 839. Springer-Verlag Berlin Heidelberg. DOI:10.1007/978-3-642-23728-7_2

ELEKTRONU PROCESI CIETĀ VIELĀ: DIRAKA IETVARS

Ē. Klotiņš

K o p s a v i l k u m s

Raksts veltīts kanoniskās Diraka teorijas modifikācijai elektronu procesu aprakstam cietā vielā. Nepieciešamā pāreja no Diraka daļiņu fizikas uz fotoierosinātu elektriski lādētu daļiņu kinētiku cietā vielā izveidota kā matemātiska struktūra, kurā ietilpst savstarpēji saistīti Hilberta telpas, kvantu lauka, un speciālās relativitātes pielietojumi. Attiecīgā fizikālā situācija ietver telpiski periodisku atomāru struktūru, kuru raksturo daļiņu dzimšana un anihilācija elektromagnētiskā lauka ietekmē. Detalizēta daļiņu dzimšana un anihilācija ilustrēta, izmantojot divu zonu modeli, kurā saglabāti arī kanoniskai Diraka teorijai raksturīgie kvantu mehānikas, speciālās relativitātes un simetrijas principi kā nepieciešamais priekšnoteikums daļiņu mijiedarbības un korelācijas kvantu kinētiskam aprakstam.

02.12.2018.

sciendo

LATVIAN JOURNAL OF PHYSICS
AND TECHNICAL SCIENCES
2019, N 1

DOI: 10.2478/lpts-2019-0007

V-FUNCTION METHOD: SOME SOLUTIONS OF DIRECT AND INVERSE DYNAMICS PROBLEMS IN A NEW STATEMENT

Nail T. Valishin
Department of Special Mathematics, Kazan National Research Technical University named after A.N. Tupolev, 10 K. Marx Str., 420111, Kazan, RUSSIA
vnailt@yandex.ru
Fan T. Valishin
Philosophy Methodology Center of Dynamism of Tatarstan Academy of Sciences, 20 Bauman Str., 420111, Kazan, RUSSIA
dinamism@yandex.ru

Based on the *V*-function method, the properties of wave nature of object motion are studied for object uniform motion with constant speed and for harmonic oscillator. It follows from the *V*-function method that object wave motion is inseparably linked with its trajectory motion. The *V*-function method consists of the principle of local variation and a new statement of the direct and inverse dynamics problems. The proposed approach made it possible to make the optico-mechanical analogy that obtained a new continuation. A comparison is made with the results obtained by Schrödinger for a harmonic oscillator.

Keywords: *optico-mechanical analogy, harmonic oscillator, variation principle, wave equation, wave function*

1. INTRODUCTION

It is known that wave-particle duality is embedded in quantum mechanics. A quantum object manifests itself as a particle in some experiments while in other ones it behaves like a wave. This duality is fixed in quantum mechanics by the Heisenberg uncertainty principle [1]. Moreover, just this circumstance makes it possible to make the optico-mechanical analogy (that still remains topical [2]–[4]) based on the existing variation principles at a level of geometrical optics only. The continuing attempts to understand the paradoxical display of wave-corpuscle duality in electron (and other microparticles) motion also promote generation of new theories developing the de Broglie's pilot-wave concept [5]–[8].

In this study, we advance a novel approach (based on the wave-corpuscle monism) to explain the quantum object nature. We propose such description of physical reality in which trajectory motion of an object is inseparably linked with its wave motion. In this case, it is assumed that particle motion is determined by

a physical wave $V(x, t)$, and presence of particle trajectories indicates the fact of particle existence.

2. MATERIALS AND METHODS

The classical approach used when developing quantum mechanics is based on description of reality using only the experimentally observed quantities. The theory developed by us is based on the process-state concept introduced to describe the essence and mode of electron existence. Such a concept is initially formulated based on the dynamism strategy [9] in which motion (process) is the essence of reality, while a trajectory (state) is the mode of reality existence. The process-state concept made it possible to formulate the principle of local variation and implement a novel statement of the direct and inverse dynamics problems [10], [11] that are components of the *V*-function method.

2.1. The V-function Method

Let us introduce a vector of the phase coordinates $x(t) = (x_1, x_2, ..., x_n)^T$; $x \in R^n$, R^n is the *n*-dimensional Euclidean space, and time $t \in T$. We consider a differential equation system:

$$\dot{x} = f(x). \tag{1}$$

The right-hand sides of $f(x)$ are vector-functions that are continuous in all their arguments. They have continuous and module limited partial derivatives $\frac{\partial f}{\partial x}$.

Variation of speed (rate) of the *V*-function change transforms the object from some state to a new state. Following is formulation of the principle of local variation: Of all the possible transitions to a new state, that one is realized at which the speed of wave function V(x, t) change takes stationary value at each instant.

$$\delta\left(\frac{dV}{dt}\right) = 0. \tag{2}$$

Let us consider the total variation of rate of wave function change:

$$\Delta\left(\frac{dV}{dt}\right) = \delta\left(\frac{dV}{dt}\right) + \frac{d}{dt}\left(\frac{dV}{dt}\right)\Delta t, \quad (\Delta t = dt), \tag{3}$$

where

$$\frac{d}{dt} = \frac{\partial}{\partial t} + \frac{\partial}{\partial x}^T \frac{dx}{dt}. \tag{4}$$

It is assumed that the wave function (V-function) is a one-valued finite piecewise continuous function satisfying the following equation:

$$\frac{\partial^2 V(x,t)}{\partial t^2} - \sum_{i,j=1}^{n} \frac{\partial^2 V(x,t)}{\partial x_i \partial x_j} f_i(x) f_j(x) = \sum_{i=1}^{n} \frac{\partial V(x,t)}{\partial x_i} \frac{df_i(x)}{dt}, \tag{5}$$

where

$f_i(x)$ are components of the n-variate vector-function of the right-hand sides of object motion Eq. (1).

Theorem I. A necessary and sufficient condition for transferring to a new state is the existence of V-function such as

$$\Delta\left(\frac{dV}{dt}\right) = 0 \cdot \tag{6}$$

Theorem II. An object motion Eq. (1) occurs so that at every instant the phase velocity vector is codirectional with the wave function gradient, i.e.,

$$\frac{\partial V}{\partial x}^T f = |\lambda \| \dot{x}| \cdot \tag{7}$$

The conclusion from Theorem II is that object motion is operated by a wave according to the de Broglie's pilot-wave concept [5], [6].

2.2. Statement of the Direct and Inverse Dynamics Problems Based on the Principle of Local Variation

The direct dynamics problem based on the V-function method is stated as follows: It is required to determine the wave function $V(x, t)$ that meets Eq. (5) from the specified differential equations describing the trajectory of object motion Eq. (1).

The edge conditions for Eq. (5) are obtained from the connectedness condition for the object wave motion with its trajectory motion and from Theorems I and II. The connectedness conditions for wave and trajectory specify the initial condition for wave function:

$$V(x,t)\big|_{t=0} = V(x,0) = 0, \tag{8}$$

and the boundary condition for wave function:

$$V(x,t)\big|_{x=0} = V(0,t) = 0 \cdot \tag{9}$$

The two other conditions result from Theorems I and II. From Theorem I

$$\Delta\left(\frac{dV}{dt}\right) = \frac{d}{dt}\left(\frac{\partial V}{\partial x}^{\mathrm{T}}\delta x\right) + \frac{d}{dt}\left(\frac{\partial V}{\partial t} + \frac{\partial V}{\partial x}^{\mathrm{T}}\dot{x}\right)dt = 0 \tag{10}$$

we get:

$$\frac{d}{dt}\left(\frac{\partial V}{\partial t}\right) = 0. \tag{11}$$

As a result, the second initial condition for Eq. (5) is as follows:

$$\left.\frac{\partial V(x,t)}{\partial t}\right|_{t=0} = \frac{\partial V(x,0)}{\partial t} = \text{const.} \tag{12}$$

The following equality results from Theorem II:

$$\frac{\partial V}{\partial x} = k^{-1}\dot{x}\cdot \tag{13}$$

The second boundary condition results from the equality Eq. (13):

$$\left.\frac{\partial V(x,t)}{\partial x}\right|_{x=0} = \frac{\partial V(0,t)}{\partial x} = k^{-1}\dot{x}(t) = k^{-1}f(x=0)\cdot \tag{14}$$

The inverse dynamics problem is specified as follows: It is required to determine differential equations of object motion (Eq. (1)) for a known wave function $V(x, t)$ that obeys Eq. (5).

For the sake of convenience, let us write Eq. (5) as follows:

$$\frac{\partial^2 V}{\partial t^2} - \dot{x}^T W\dot{x} = \frac{\partial V}{\partial x}^T\frac{d\dot{x}}{dt}, \quad W = \left[\frac{\partial^2 V(x,t)}{\partial x_i \partial x_j}\right]. \tag{15}$$

Knowing the wave function $V(x, t)$, we obtain from Eq. (7) solution of the inverse dynamics problem as

$$\dot{x}_i = k\frac{\partial V}{\partial x_i}\cdot \tag{16}$$

It can be shown from Eq. (10) and Theorem II that the following equality takes place:

$$\frac{\partial V}{\partial x}^T \frac{d}{dt}\dot{x} = 0 \cdot \tag{17}$$

As a result, Eq. (15) becomes

$$\frac{\partial^2 V}{\partial t^2} - \dot{x}^T W \dot{x} = 0 \cdot \tag{18}$$

The above results are used to make the optico-mechanical analogy and simulate trajectory-wave motion of a harmonic oscillator.

3. RESULTS AND DISCUSSION

3.1. Solving the Direct and Inverse Dynamics Problems

Let us consider solving the direct and inverse dynamics problems for object uniform motion with constant speed. In this case, Eqs. (1) and (5) are:

$$\dot{x} = \vartheta \tag{19}$$

$$\frac{\partial^2 V}{\partial t^2} - \dot{x}^2 \frac{\partial^2 V(x,t)}{\partial x^2} = 0, \tag{20}$$

With allowance made for Eq. (19), we obtain from Eq. (20) the classical wave equation:

$$\frac{\partial^2 V}{\partial t^2} - \vartheta^2 \frac{\partial^2 V(x,t)}{\partial x^2} = 0, \tag{21}$$

for which the conditions Eqs. (8) and (9) remain invariant, while Eqs. (12) and (14) become:

$$\left.\frac{\partial V(x,t)}{\partial t}\right|_{t=0} = \frac{\partial V(x,0)}{\partial t} = \widetilde{C}_1, \tag{22}$$

$$\left.\frac{\partial V(x,t)}{\partial x}\right|_{x=0} = \frac{\partial V(0,t)}{\partial x} = \widetilde{C}_2 \cdot \tag{23}$$

To solve Eq. (21) with the specified edge conditions, we apply the variable separation method $V(x,t) = \varphi(t)\psi(x)$:

$$\frac{\ddot{\varphi}(t)}{\varphi(t)} = \vartheta^2 \frac{\psi''(x)}{\psi(x)} = -\omega^2$$
$$\ddot{\varphi}(t) + \omega^2 \varphi(t) = 0 \quad . \tag{24}$$
$$\psi''(x) + \frac{\omega^2}{\vartheta^2}\psi(x) = 0$$

As a result, the general solution of Eq. (21) is as follows:

$$V(x,t) = \left(C_1 e^{-i\omega t} + C_2 e^{i\omega t}\right)\left(C_3 e^{-i\frac{\omega}{\vartheta}x} + C_4 e^{i\frac{\omega}{\vartheta}x}\right). \tag{25}$$

The constants in Eq. (25) will be expressed through the initial and boundary conditions Eqs. (8), (9) and (23), i.e.,

$$\varphi(0)\psi(x) = C_1 + C_2 = 0$$
$$\dot{\varphi}(0)\psi(x) = \left(-i\omega C_1 + i\omega C_2\right)\psi(x) = \widetilde{C}_1 \Rightarrow \dot{\varphi}(0) = \overline{C}_1$$
$$\varphi(t)\psi(0) = C_3 + C_4 = 0 \quad . \tag{26}$$
$$\varphi(t)\psi'(0) = \varphi(t)\left(\frac{-i\omega}{\vartheta}C_3 + \frac{i\omega}{\vartheta}C_4\right) = \widetilde{C}_2 \Rightarrow \psi'(0) = \overline{C}_2$$

It follows from Eq. (26) that:

$$C_1 = -C_2, C_2 = \frac{\overline{C}_1}{i\omega}$$
$$C_3 = -C_4, C_4 = \frac{\vartheta\overline{C}_2}{i\omega} \quad . \tag{27}$$

By substituting the obtained constants into Eq. (25), we get:

$$V(x,t) = \left(\frac{-\overline{C}_1}{i\omega}e^{-i\omega t} + \frac{\overline{C}_1}{i\omega}e^{i\omega t}\right)\left(\frac{-\vartheta\overline{C}_2}{i\omega}e^{-i\frac{\omega}{\vartheta}x} + \right.$$
$$\left. + \frac{\vartheta\overline{C}_2}{i\omega}e^{i\frac{\omega}{\vartheta}x}\right) = -\frac{\vartheta\overline{C}_2\overline{C}_1}{\omega^2}e^{-i(\omega t + \frac{\omega}{\vartheta}x)} + \frac{\vartheta\overline{C}_2\overline{C}_1}{\omega^2}e^{i(\omega t - \frac{\omega}{\vartheta}x)} + \quad . \tag{28}$$
$$+ \frac{\vartheta\overline{C}_2\overline{C}_1}{\omega^2}e^{-i(\omega t - \frac{\omega}{\vartheta}x)} - \frac{\vartheta\overline{C}_2\overline{C}_1}{\omega^2}e^{i(\omega t + \frac{\omega}{\vartheta}x)} =$$
$$= -\frac{\vartheta\overline{C}_2\overline{C}_1}{\omega^2}e^{\pm i(\omega t + \frac{\omega}{\vartheta}x)} + \frac{\vartheta\overline{C}_2\overline{C}_1}{\omega^2}e^{\pm i(\omega t - \frac{\omega}{\vartheta}x)}$$

The solution is in the form of a plane wave. In what follows we consider wave propagation only in the direction of object motion. Then from Eq. (28) we get the *V*-function as

$$V(x,t) = \frac{\vartheta \overline{C}_2 \overline{C}_1}{\omega^2} e^{\pm i(\frac{\omega}{\vartheta}x - \omega t)} = Ae^{\pm i(\frac{\omega}{\vartheta}x - \omega t)}. \tag{29}$$

3.2. Continuation of the Optico-mechanical Analogy

Based on the inverse dynamics problem, one can see that the trajectory motion of a particle (at $n = 1$), as follows from Eq. (16), has to satisfy Eq. (20):

$$\dot{x} = k\frac{\partial V}{\partial x}. \tag{29}$$

Thus, all this makes it possible to draw the following analogy between wave and particle:

$$\begin{aligned} &\vartheta = \vartheta, \ \omega = \frac{m\vartheta^2}{\hbar} = \frac{2E}{\hbar}, \\ &\lambda = \frac{h}{m\vartheta}, \ A = \hbar. \end{aligned} \tag{30}$$

It follows from the first relation in Eq. (30) that wave phase velocity is equal to particle velocity. It is known from quantum mechanics that group velocity of the de Broglie waves is equal to particle velocity. The second relation in Eq. (30) shows relationship between particle energy and wave carrier frequency. Based on the third relation in Eq. (30), the wavelength λ is determined by the particle momentum. And this relation coincides with the famous de Broglie relation. As a result, particle position is determined by the wave node. In this case, wave guides particle; at the same time, particle generates wave.

3.3. A Linear Harmonic Oscillator

Let us consider a linear harmonic oscillator. From Eq. (31) of trajectory motion of object (particle):

$$m\ddot{x} = -kx. \tag{31}$$

The trajectory motion of object (particle) is joined with wave motion described by Eq. (23) and at $n = 1$ is:

$$\frac{\partial^2 V}{\partial t^2} - \dot{x}^2 \frac{\partial^2 V(x,t)}{\partial x^2} = 0. \tag{32}$$

As a result, we get solution as a function of time:

$$x(t) = \frac{\vartheta_0}{\omega_0} \sin \omega_0 t, \tag{33}$$

where

$$\omega_0 = \sqrt{\frac{k}{m}}. \tag{34}$$

The object motion speed will be determined from time derivative of this solution.

In our case, separation of variables is performed in such a way:

$$\frac{\ddot{\varphi}(t)}{\dot{x}^2(t)\varphi(t)} = \frac{\psi''(x)}{\psi(x)} = -\frac{1}{\lambda^2}, \tag{35}$$

where λ is a constant. For this we have:

$$\psi''(x) + \frac{1}{\lambda^2}\psi(x) = 0, \tag{36}$$

$$\ddot{\varphi}(t) + \frac{\dot{x}^2(t)}{\lambda^2}\varphi(t) = 0. \tag{37}$$

Let us introduce the dimensionless quantity $\tau = \sqrt{\omega_0 \omega t}$; as a result, we obtain:

$$\ddot{\varphi}(\tau) + \frac{\vartheta_0^{\,2}}{\omega^2 \lambda^2}\left(\frac{\omega}{\omega_0} - \tau^2\right)\varphi(\tau) = 0. \tag{38}$$

Thus, it follows from Eq. (38) that for harmonic oscillator when the object motion speed as a function of time and object motion trajectory are known and wave function is superimposed on the trajectory, we get discrete energy values, just as in the Schrödinger case [12], [13] for harmonic oscillator.

Now let us apply the *V*-function method:

$$\dot{x}^2 = \frac{2E - kx^2}{m}. \tag{39}$$

With allowance made for Eq. (39) it becomes:

$$\frac{\partial^2 V}{\partial t^2} - \left(\frac{2E - kx^2}{m} \right) \frac{\partial^2 V}{\partial x^2} = 0 \cdot \tag{40}$$

The following equations are obtained from Eq. (40) after separation of variables:

$$\varphi'' + \omega^2 \varphi = 0 , \tag{41}$$

$$\psi'' + \frac{m\omega^2}{2E - kx^2} \psi = 0 \cdot \tag{42}$$

Let us introduce a dimensionless quantity $\xi = \frac{x}{\sqrt{\frac{2E}{k}}}$; then Eq. (42) is:

$$\psi'' + \frac{\eta^2}{1 - \xi^2} \psi = 0 , \tag{43}$$

where

$$\eta^2 = \frac{m\omega^2}{k} = \frac{\omega^2}{\omega_0^2} . \tag{44}$$

We apply the computer mathematics system Maple to solve Eq. (43). Its solution is:

$$\psi(\xi) = C_1 (\xi - \xi^3) \text{hypergeom}\left(\left[\frac{5}{4} + \frac{1}{4}\sqrt{4\beta^2 + 1} \right], \left[\frac{5}{4} - \frac{1}{4}\sqrt{4\beta^2 + 1} \right], \left[\frac{3}{2} \right], \xi^2 \right) \cdot \tag{45}$$

The solution of Eq. (42) in this system is as a series:

$$\begin{aligned} \psi(x) = \frac{1}{E} C_1 x (E - \frac{kx^2}{2})(1 + \frac{1}{12} \frac{6k - m\omega^2}{E} x^2 + \frac{1}{480} \frac{(6k - m\omega^2)(20k - m\omega^2)}{E^2} x^4 + \\ \frac{1}{40320} \frac{(6k - m\omega^2)(20k - m\omega^2)(42k - m\omega^2)}{E^3} x^6 + \\ \frac{1}{5806080} \frac{(6k - m\omega^2)(20k - m\omega^2)(42k - m\omega^2)(72k - m\omega^2)}{E^4} x^8 + \ldots) \end{aligned} \cdot \tag{46}$$

It follows from Eq. (46) that continuous solution $\psi(x)$ has to satisfy the condition $\psi\left(x=\sqrt{\frac{2E}{k}}\right)=0$ This condition is fulfilled only at certain discreet values of proper frequencies: $\eta_1^2=\frac{\hbar^2\omega_1^2}{\hbar^2\omega_0^2}=6,\ \eta_2^2=\frac{\hbar^2\omega_2^2}{\hbar^2\omega_0^2}=20,\ \eta_3^2=\frac{\hbar^2\omega_3^2}{\hbar^2\omega_0^2}=42,\ \eta_4^2=\frac{\hbar^2\omega_4^2}{\hbar^2\omega_0^2}=72,\ldots$.

From this we get the following rule of energy quantization for harmonic oscillator:

$$E_{n+2}^2-2E_{n+1}^2+E_n^2=\Delta\ \ E_n^2=2\hbar^2\omega_0^2\,. \tag{47}$$

Therefore, when the trajectory motion of an object is closely related to the wave motion, the harmonic oscillator energy can have, as in the Schrödinger case, only certain discrete values: $E_1^2=6\hbar^2\omega_0^2, E_2^2=20\hbar^2\omega_0^2, E_3^2=42\hbar^2\omega_0^2, E_4^2=72\hbar^2\omega_0^2\ldots$.

In this case, if the results obtained by Schrödinger ($E_n=\left(n+\frac{1}{2}\right)\hbar\omega_0$) are substituted into equality Eq. (47), then we have:

$$\left(\left(n+2+\frac{1}{2}\right)^2-2\left(n+1+\frac{1}{2}\right)^2+\left(n+\frac{1}{2}\right)^2\right)\hbar^2\omega_0^2=2\hbar^2\omega_0^2\,, \tag{48}$$

i.e., we get an identity. It is known [14], [15] that in real microscopic oscillators interacting with light only transitions between the adjacent levels can occur.

It should be noted that a Wronskian for Eq. (43) is a nonzero constant, i.e., from this we get the second linearly independent solution

$$\frac{\psi_n(\xi)\widetilde{\psi}_n'(\xi)-\widetilde{\psi}_n(\xi)\psi_n'(\xi)}{(\psi_n(\xi))^2}=\left(\frac{\widetilde{\psi}_n(\xi)}{\psi_n(\xi)}\right)'=\frac{\tilde{N}}{(\psi_n(\xi))^2}\quad\Rightarrow \tag{49}$$

$$\widetilde{\psi}_n(\xi)=C\psi_n(\xi)\int\frac{1}{(\psi_n(\xi))^2}d\xi\,. \tag{50}$$

It follows from relations that $|\psi_n(\xi)|\to\infty$ as $\xi\to\infty$. Thus, we obtain from Eq. (50) that $\widetilde{\psi}_n(\xi)\to 0$ as $\xi\to\infty$, i.e., the solution is finite at infinity.

4. CONCLUSIONS

Using the *V*-function method, we get that particle uniform motion with constant speed is joined with wave motion. The obtained wave function has to

satisfy the classical wave equation. In this case, if the wave function (V-function) has dimension of action ([kg][m/s][m]), then particle energy takes certain discrete values. The quantization law becomes the same as the Schrödinger energy quantization law for harmonic oscillator.

Thus, based on the V-function method, any trajectory motion of an object is inseparably linked with its wave motion. We have considered both direct and inverse problems for the case of particle uniform motion with constant speed. The opto-mechanical analogy is made and accordance between wave and particle is obtained. Here the main factor is equality of phase speed of wave and speed of particle motion.

In the case of harmonic oscillator when trajectory motion of particle is not related to wave motion, the Schrödinger equation for harmonic oscillator results. If trajectory equation is inseparably linked with wave equation, then we get the energy quantization rule linking three adjacent levels. This is in agreement with the real microscopic oscillators interacting with light. The finite solutions for harmonic oscillator are also obtained.

REFERENCES

1. Heisenberg, W. (1930). *Die Physikalischen Prinzipien der Quantentheorie*. Leipzig: Springer.
2. Bloch, A.M., & Rojo, A.G. (2016). Optical mechanical analogy and nonlinear nonholonomic constraints. *Physical Review E*, *93*(2), 023005. DOI: 10.1103/PhysRevE.93.023005
3. Abdil'din, M.M., Abishev, M.E., Beissen, N.A., & Taukenova, A.S. (2011). On the optical-mechanical analogy in general relativity. *Gravitation and Cosmology*, *17*(2), 143–146.
4. Khan, S.A. 2017. Hamilton's optical-mechanical analogy in the wavelength-dependent regime. *Optik - International Journal for Light and Electron Optics*, *130*, 714–722.
5. De Broglie, L. (1967). Waves and quanta. Quanta of light, diffraction and interference. Quanta, the kinetic theory of gases and the Fermat principle. *Advances of Physical Sciences*, *93*(1), 178–180.
6. De Broglie, L. (1986). *The Heisenberg uncertainty relations and the probabilistic interpretation of wave mechanics*. Moscow: Mir.
7. Böhm, D. (1951). *Quantum Theory*. Englewood Cliffs: Prentice-Hall.
8. Knoll, Y., & Yavneh, L. (2006). *Coupled wave-particle dynamics as a possible ontology behind Quantum Mechanics and long-range interactions*. *arXiv:quant-ph/0605011*. Available at: http://citeseerx.ist.psu.edu/viewdoc/download?doi=10.1.1.252.7980&rep=rep1&type=pdf
9. Valishin, F.T. (2018). *The problem of the beginning and the strategy of dynamism*. Moscow: Entsiklopedist-Maksimum.
10. Valishin, N.T. (2014). Variational principle and the problems dynamics. *Life Science Journal*, *11*(8), 568–574.
11. Valishin, N.T. (2016). An optical-mechanical analogy and the problems of the trajectory-wave dynamics. *Global Journal of Pure and Applied Mathematics*, *12*(4), 2935–2951.
12. Schrödinger, E. (1926). Quantisierung als Eigenwertproblem. *Annalen der Physik*, *384*(4), 361–376.

13. Schrödinger, E. (1959). Quantization as a problem of eigenvalues. In: *Variational Principles of Mechanics. Digest of Articles* (pp. 668–704). Moscow: Fizmatgiz.
14. Goldin, L.L., & Novikova, G.I. (2002). *Quantum physics. Introductory course*. Moscow: Institute for Computer Research.
15. Syzrantsev, V.N., Chelombitko, S.I., & Gammer, M.D. (2018). The use of virtual laboratory works in the study of engineering disciplines of oil and gas training. *Periódico Tchê Química*, *15*(30), 563–570.

V-FUNKCIJAS METODE: DAŽI TIEŠĀ UN APGRIEZTĀ DINAMIKAS UZDEVUMU RISINĀJUMI JAUNĀ IZKLĀSTĀ

N. T. Vališins, F. T. Vališins

K o p s a v i l k u m s

Pamatojoties uz V-funkcijas metodi, objekta kustības viļņu rakstura īpašības pētītas objekta vienādas kustības ar nemainīgu ātrumu un harmoniskā oscilatora mērķim. No V-funkcijas metodes izriet, ka objekta viļņu kustība ir nesaraujami saistīta ar trajektorijas kustību. V-funkcijas metode iekļauj vietējās variācijas principu un jaunu tiešā un apgrieztā dinamikas uzdevumu izklāstu. Ierosinātā pieeja ļāva veikt optisko un mehānisko analoģiju, kas ieguva jaunu turpinājumu. Salīdzinājums veikts ar rezultātiem, ko Šrēdingers ieguva attiecībā uz harmonisko oscilatoru.

17.12.2018.